water

MDPI

Article

TiO_2/Activated Carbon/2D Selenides Composite Photocatalysts for Industrial Wastewater Treatment

Shehzad Ahmad [1,*], Muhammad Suleman Tahir [2,3], Ghulam Mustafa Kamal [1,4], Xu Zhang [5,6,7,*], Saima Nazir [4,8], Muhammad Bilal Tahir [9], Bin Jiang [5,6,7] and Muhammad Safdar [1]

1 Institute of Chemistry, Khwaja Fareed University of Engineering and Information Technology, Rahim Yar Khan 64200, Pakistan
2 Institute of Chemical and Environmental Engineering, Khwaja Fareed University of Engineering and Information Technology, Rahim Yar Khan 64200, Pakistan
3 Department of Chemical Engineering, University of Gujrat, Gujrat 50700, Pakistan
4 Institute of Health Sciences, Khwaja Fareed University of Engineering and Information Technology, Rahim Yar Khan 64200, Pakistan; saimasalman50@yahoo.com
5 Optics Valley Laboratory, Wuhan 430074, China
6 State Key Laboratory of Magnetic Resonance and Atomic Molecular Physics, Key Laboratory of Magnetic Resonance in Biological Systems, National Center for Magnetic Resonance in Wuhan, Wuhan Institute of Physics and Mathematics, Innovation Academy for Precision Measurement Science and Technology, Chinese Academy of Sciences, Wuhan 430074, China
7 Wuhan National Laboratory for Optoelectronics, Huazhong University of Science and Technology, Wuhan 430071, China
8 Nawaz Sharif Medical College, University of Gujrat, Gujrat 50700, Pakistan
9 Institute of Physics, Khwaja Fareed University of Engineering and Information Technology, Rahim Yar Khan 64200, Pakistan
* Correspondence: shehzad17151@gmail.com (S.A.); zhangxu@wipm.ac.cn (X.Z.)

Abstract: Even in the 21st century, water contamination has been a big problem and industrial processes are to be blamed for polluted water supplies. The use of sunlight in the process of photocatalysis is an efficient way to purify wastewater. Composites of TiO_2/activated carbon/two-dimensional selenides performed better than either of the individual material or binary composites for this application. A straightforward hydrothermal technique was employed in the synthesis of photocatalysts. The synthesized photocatalytic composites were verified with the help of UV-Visible spectroscopy, FTIR, XRD, and SEM. The heterostructures absorbed nearly all of the sun's UV and visible light. These photons are then converted into usable reducing electrons and oxidizing species such as $^{\bullet}O_2$ and $OH^{\bullet}$ to decompose organic pollutants from industrial wastewater. Since there were additional pathways available for charge transfer along with several active edge sites, the composite photocatalysts are proven more active than individual TiO_2 and 2D $MoSe_2$ components. With the help of a cascade-driven mechanism of electrons, these channels can transmit more charges than single-component heterojunctions. The results provided a realistic method for developing photocatalyst composites powered by solar light for use in industrial wastewater treatment. Results of degradation of methylene blue suggest that the synthesized composites possess better photocatalytic activity. This enhanced photocatalytic activity is not limited to organic dyes. Other hazardous organic pollutants present in industrial wastewater can be decomposed by using this approach.

Keywords: TiO_2/activated carbon; 2D selenides; photocatalyst; wastewater treatment

Citation: Ahmad, S.; Tahir, M.S.; Kamal, G.M.; Zhang, X.; Nazir, S.; Tahir, M.B.; Jiang, B.; Safdar, M. TiO_2/Activated Carbon/2D Selenides Composite Photocatalysts for Industrial Wastewater Treatment. *Water* **2023**, *15*, 1788. https://doi.org/10.3390/w15091788

Academic Editors: Christos S. Akratos and Gongduan Fan

Received: 27 March 2023
Revised: 24 April 2023
Accepted: 3 May 2023
Published: 6 May 2023

1. Introduction

Water is essential for every individual to sustain life on earth [1]. Rapidly growing populations, urbanization, extensive agricultural practices and industrialization are the main reasons for water pollution, a threatening issue of the modern world [2–4]. In the previous decade, a rapid increase in industries and industrial processes have created a

huge impact in water pollution [5]. Industrial waste materials are the most frightening environmental issues. They impose serious health effects on humans via surface wastewater bodies [6,7]. About 2.2 million people die annually due to waterborne diseases in developing countries [8]. The consumption of contaminated water causes diarrhea and approximately 1.8 million children lose their lives every year from this disease [9,10]. There is an urgent need to minimize the problem of water pollution and to save human beings and aquatic life from these chronic diseases.

Water treatment facilities are preventive measures against waterborne diseases [11]. A huge amount of water is used in textile industries for different processes. Water is used for washing purposes in the industry. If this water is released as such without treatment, it imposes a serious threat on ecosystem [12]. This water is contaminated with animal oils, fiber lint, organic dyes and other hazardous chemicals. These chemicals are used to improve the quality of raw material. The liquid wastes along with several contaminants are discarded from these industries, causing environmental pollution [13,14]. The colored wastewater of these industries contains an unpleasant odor, chemical oxygen demand, biochemical oxygen demand, high pH and suspended solids. Suspended solids are composed of different inorganic salts, heavy metals and hazardous chemicals [15,16]. A high concentration of carcinogenic organic dyes is also present in industrial effluents [17]. Synthetic dyes can cause genetic mutations and cancer in human beings. These organic dyes enter the food chain from wastewater of the textile industry. Dyes are extensively used in the textile industry in different processes [18]. Textile industries are responsible for one-fifth of industrial water pollution worldwide [19]. Methylene blue (MB) is the most commonly used dye in textile industry. A large amount of MB is released in wastewater from textile industries [20]. Above a certain concentration it is harmful for human beings, microbes and the environment. MB is responsible for blindness, abdominal disorders, digestive and destructive disorders [21,22]. It also causes diarrhea, cyanosis, gastritis, jaundice, methemoglobinemia, shock, skin and eye irritation, tissue necrosis and vomiting [20].

Many conventional techniques such as biological treatments, adsorption, filtration, sedimentation, osmosis, reverse osmosis and chemical treatments are applied for water purification. Conventional techniques have been applied for the removal of contaminants from wastewater, thereby enhancing water quality. These techniques are not adequately effective to clean wastewater containing diverse contaminants [23]. The urgent need of the time is to develop alternative wastewater techniques. The techniques which are capable of completely eliminating these hazardous contaminants from wastewater are always preferred [24].

Advanced oxidation processes are recently revolutionized as wastewater treatment technique. These produce highly reactive free radicals ($^{\bullet}OH$) by degrading inorganic and organic pollutants. $^{\bullet}OH$ free radicals oxidize carbonaceous species into inorganic ions and CO_2 gas, a product due to their strong oxidizing nature [25]. Oxidants such as ozone and hydrogen peroxide can trigger the formation of $^{\bullet}OH$. This can be completed by using energy resources such as heat, ultrasounds and ultraviolet light or by using homogeneous or heterogeneous photocatalysts such as Fenton's reagent, TiO_2 or ZnO [26]. Among these advanced oxidation processes, a photocatalytic oxidation process is an attractive technique. In this process, impurities and pollutants can be eliminated with the help of oxidation activated by free radicals at a normal temperature and pressure. This results in non-selective oxidation of contaminants in water such as carbon dioxide, anions and cations. $^{\bullet}OH$, free radicals possess very high oxidation potential ($^{\bullet}OH/H_2O$) = 2.80 eV/SHE. It is the second most proficient oxidation potential. Maximum oxidation potential carries fluorine (E° = 3.0 eV) [27]. Free radicals have a very short lifespan in water and vanish rapidly from reaction medium [28]. The prime drawbacks of traditional advanced oxidation processes include the following: tedious instrumentation, inadequate mineralization of pollutants/contaminants, high-cost processing, ultraviolet light activity and half-life time of O_3 [29–31].

Semiconductor-material-based photocatalysts have been proven as the best solution to cover these drawbacks. Semiconductor photocatalysts do not form any kind of secondary pollutants in water. Because of their chemically stable nature, photocatalysts can be reprocessed in aqueous medium [32]. TiO_2 has been an extensively studied semiconducting material, in the previous decade. Its wide applications are due to its easy availability, low price and non-poisonous character, high stability, porous structure and greater surface area [33–35].

Major limitations of TiO_2 include suppression of photocatalytic activity, slow photocatalytic degradation rates, higher band energy, and aggregation of TiO_2 nanoparticles due to unstable nanosized particles [36–39]. Photocatalytic properties of TiO_2 can be increased in a visible region by minimizing a quick recombination of the photogenerated charge carrier, by depositing metal nanoparticles on its surface [40–42].

A very effective strategy to expand absorption in the visible range from UV solar light and to enhance photo-induced charge separation is the construction of heterostructure [43,44]. For this purpose, transition metal semiconductors can increase the photo-induced charge separation of TiO_2 and their $Mn^+/M^{(n-1)+}$ (M = transition metal) cycle directly activates persulphates to reduce pollutants in wastewater [45]. In addition to the limitations of semiconductors, major hindrances in the practical applications of composites include ion diffusion, slow charge transfer and deficient electromagnetically active sites [46].

In recent research, two-dimensional transition metal dichalcogenides have grasped the attention of researchers due to their unique electronic and optical properties. These materials possess excellent light absorbance and fast electron migrating properties [47]. A large number of active sites on their crystal edges provide more surface area for photocatalytic reaction. Therefore, transition metal dichalcogenides are predictably suitable co-catalysts for TiO_2, to reduce its carrier recombination and improve its light absorbance capacity [48–50]. For example, $MoSe_2$, has been proven to be a promising semiconductor because of its narrow band gap (1.7 to 1.9 eV), which absorbs a broader range of solar light [51]. It contains better antiphotocorrosive stability and an exceptional two-dimensional (2D) layer structure for surface reaction [52–54]. In 2D $MoSe_2$, Mo atoms are entrapped between the layers of Se atoms via van der Waals cohesive forces [55]. The layered structure of 2D $MoSe_2$ can be referenced from a recent study which proved that interlayer spacing of MoS_2 can be expanded in different phases [56]. The lower cost of $MoSe_2$ and easy availability proves it is a better cocatalyst than the graphene and noble metals [48,57].

Carbon materials are used to modify TiO_2 because of their excellent electrical conductivity and strong visible light absorbing property. These properties enhance the efficiency of photo-induced carrier separation [58,59]. Activated carbon (AC) is the most promising adsorbent. The large surface area of AC, high surface activity and highly porous structure enhance its absorption character. Different varieties of activated carbon are used as adsorbents, catalysts and catalyst supporters [60]. Literature survey regarding publications on relevant topic has been given in Table 1.

Table 1. No. of publications on $TiO_2/MoSe_2$ from 2019 to 2023 at different sources.

Sr. No.	Source	No. of Publications in Years					
		2019	**2020**	**2021**	**2022**	**2023**	**2019–2023**
1	Google Scholar	545	783	951	1580	668	4527
2	Science Direct	6	6	20	15	10	57

TiO_2/Activated Carbon/2D-Selenide photocatalysts were synthesized using the simple hydrothermal method. These composites absorb broad spectrum solar light in the ultraviolet, visible and NIR region due to the presence of 2D $MoSe_2$. The 2D $MoSe_2$ reduces the band gap of TiO_2 and AC increases the light absorption tendency of TiO_2. Maximum light absorption power and the reduced band gap proves TiO_2/AC/2D$MoSe_2$ a better photocatalyst for degradation of organic hazardous pollutants in wastewater.

2. Materials and Methods

2.1. Materials

Charcoal (C), polyethylene glycol (C_2nH4n+_2On+1), ethylene diamine tetra acetic acid ($[CH_2N(CH_2CO_2H)_2]_2$), sodium selenite (Na_2O_3Se), hydrazine (N_2H_4), ammonium paramolybdate tetrahydrate ($(NH_4)_6Mo_7O_{24}.4H_2O$), and other reagents were imported from Sigma-Aldrich. All the chemicals were of analytical grade so there was no need to further purify them.

2.2. Activation of Charcoal

Sequence wise procedure for the activation of carbon has been shown in Figure 1. A total of 3 g of charcoal was dipped completely into 1 M hydrochloric acid and left for 24 h. After that the mixture was stirred for 2 h at 25 °C, filtered, and washed with distilled water, 0.1 M sodium hydroxide (NaOH) and again with distilled water. The activated carbon was then dried and saved for further use.

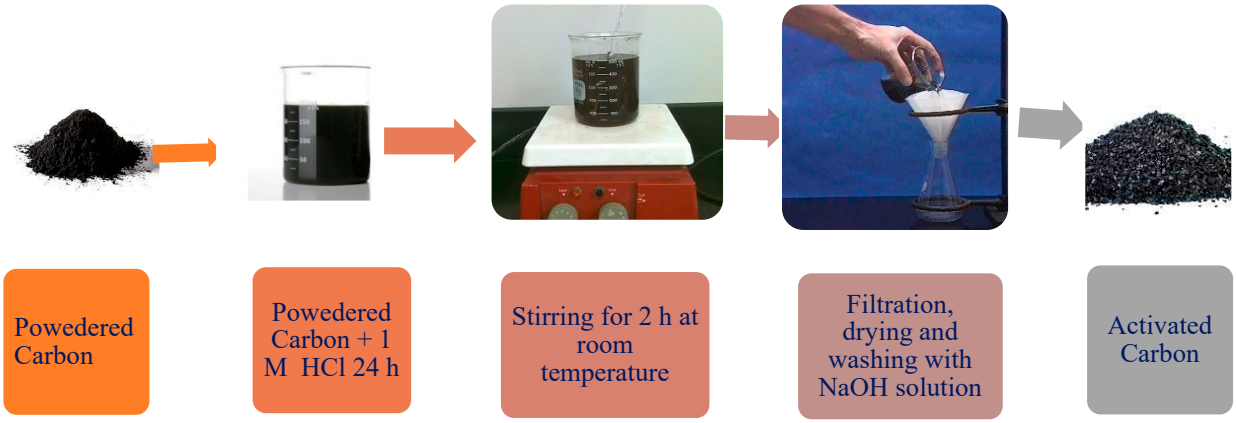

Figure 1. Schematic representation of activation of carbon.

2.3. Synthesis of TiO_2

Schematic representation of the synthesis of TiO_2 has been shown in Figure 2. TiO_2 was synthesized using the hydrothermal method [53]. Then, 20 mL of titanium tetra butoxide ($C_{16}H_{36}O_4Ti$) was added in excess of 0.1 M NaOH by continuous stirring. The pH of this solution was decreased from 8–9 to 2–3 by adding 0.1 M HCl. The mixture was added into a Teflon-lined autoclave, screwed tightly and kept in an oven at 170 °C for 24 h. Precipitates of TiO_2 were obtained, filtered, washed with methanol (CH_3OH) and distilled water, and dried. Annealing of TiO_2 crystals was conducted at 300 °C for 3 h and then saved for further use.

2.4. Synthesis of $TiO_2/_xAC/2DMoSe_2$

Schematic representation of synthesis of $TiO_2/_xAC/2D$ $MoSe_2$ has been shown in Figure 3 $TiO_2/_xAC/2DMoSe_2$ heterostructures were prepared as follows. In the first step, 2D $MoSe_2$ was prepared by adding 15 mL of polyethylene glycol (PEG) in 15 mL of distilled water while stirring continued. The solution was divided into two equal halves into beaker A and B. Then, 1–2 drops of ethylene diamine along with 0.359 g of sodium selenite and 5 mL of hydrazine along with 0.176 g ammonium paramolybdate tetrahydrate were added in beaker A and B, respectively, by constant stirring. Both the mixtures were stirred for 30 min and mixed into beaker C by continuous stirring for 10 min. In the second step, $TiO_2/_xAC/MoSe_2$ was prepared by adding 1% (by mass) of TiO_2 and activated carbon into the above mixture. The mixture was magnetically stirred for 20 min and then transferred into a 100 mL autoclave. After, the airtight sealed autoclave was placed in an oven for 24 h at 200 °C. The precipitates obtained were washed with methanol, distilled water, and dried at 60 °C overnight. The resulting composites were given the name of $TiO_2/_xAC/MoSe_2$.

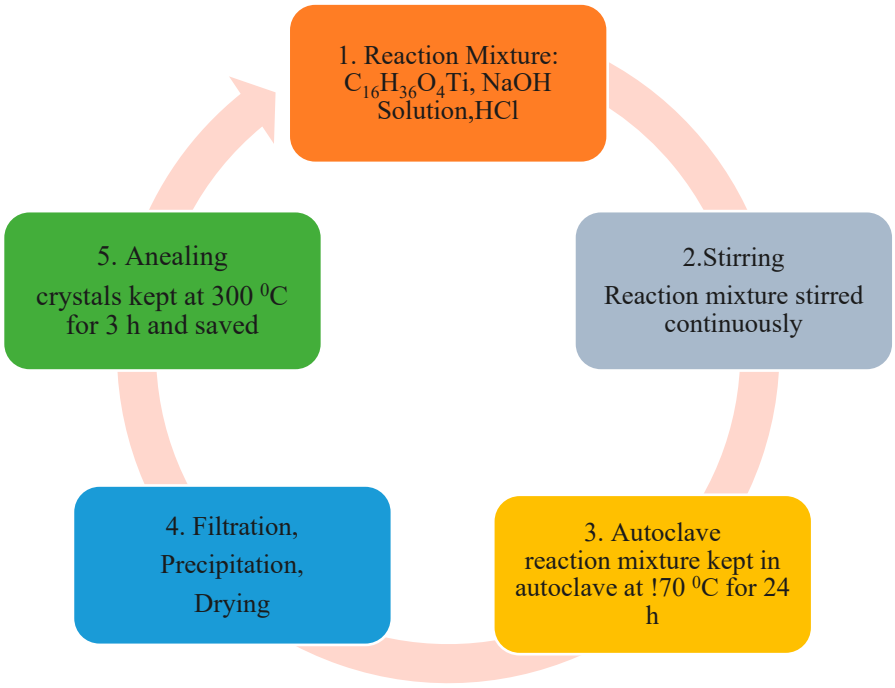

Figure 2. Schematic representation of stepwise synthesis of TiO_2.

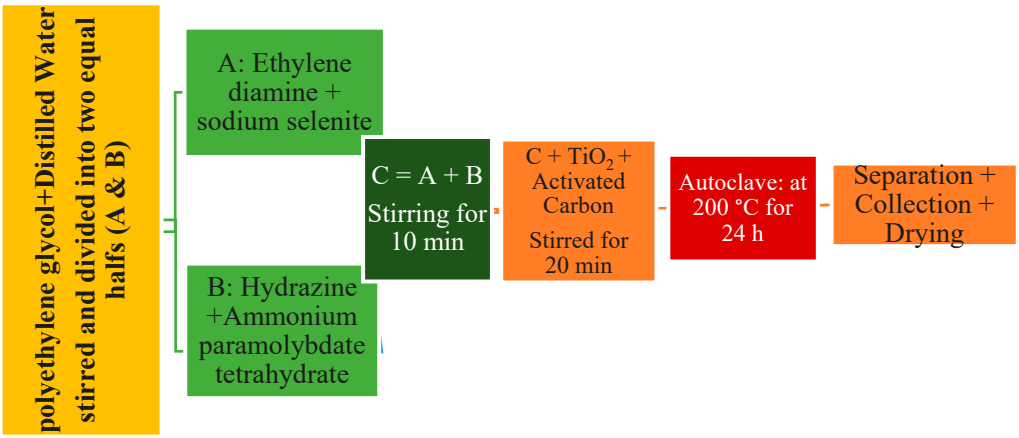

Figure 3. Schematic representation of stepwise synthesis of TiO_2/ AC/$2DMoSe_2$.

The samples of 0.25%, 0.5%, 0.75% and 100% by mass ratios of activated carbon were denoted as $TiO_2/_{0.25}AC/2DMoSe_2$, $TiO_2/_{0.5}AC/2DMoSe_2$, $TiO_2/_{0.75}AC/2DMoSe_2$ and $TiO_2/_1AC/2DMoSe_2$, respectively.

2.5. Characterization

A PerkinElmer 100 FT-IR spectrometer (Waltham, MA, USA) was used to record FTIR spectra of synthesized composites. The range of the FTIR spectrometer was set at 400–4500 cm^{-1} in transmittance mode in the Hi-Tech Laboratory of KFUEIT Rahim Yar Khan, Pakistan. The XRD studies were performed at the University of Peshawar, Pakistan by using the JEOL X-ray diffractometer (Model: JDX-3532, JEOL, Tokyo Japan). X-rays of CuKα with Wavelength = 1.5418 Å and 2Theta-Range: 0 to 160°. The SEM characterization was performed in the Central Resource Laboratory of the University of Peshawar Pakistan by using SEM (Model: JSM 5910, JEOL, Tokyo Japan). UV-Visible spectroscopy was performed in the laboratory of the Institute of Chemical & Environmental Engineering, KFUEIT Rahim Yar Khan Pakistan. Quartz cuvettes were used as a sample holder. Distilled water was used as a reference.

3. Results and Discussion

3.1. FTIR Study of Composites

In FTIR spectra, peaks at 830 cm^{-1}, 1090 cm^{-1}, 2941 cm^{-1} and 3650 cm^{-1} were representing O-Mo-O, Se-O bond, C-H stretching and OH stretching, respectively (Figure 4) [61,62]. Bands in the range of 550–750 cm^{-1} ascribe a stretching vibration of the O-Ti bond [63]. The absorption peak at 3410.51 cm^{-1} shows -OH stretching vibration. This stretching peak shows absorption of water molecules, alcohols and phenolic compounds on the surface of photocatalyst [64,65]. The peak at 1600.89 cm^{-1} is of C=C aromatic ring stretching vibration, shifted from 1634 cm^{-1} to 1600.89 cm^{-1}. Peaks that appeared at 832 cm^{-1} and 600 cm^{-1} show the formation of oxygen metal bonding. Therefore, these peaks represent the titanium dioxide loaded with activated carbon [66]. The band between 550 and 650 cm^{-1} shows a stretching vibration of Ti-O. At 1060.43 cm^{-1} a peak indicates activated carbon. The peak intensity at 1060 cm^{-1} increases with an increase in activated carbon. An absorption peak at 949 cm^{-1} and 550 cm^{-1} represents O-Ti-O-C bonds [67]. It was ascribed to the titania mixture described by Zhang et al. A peak present at 1060.43 cm^{-1} shows the C-O-Ti bond. A minute conjugation of Ti-O and a bulk of activated carbon is due to the electron affinity difference [68]. At 1060 cm^{-1} the peak shows the Se-O bond [14].

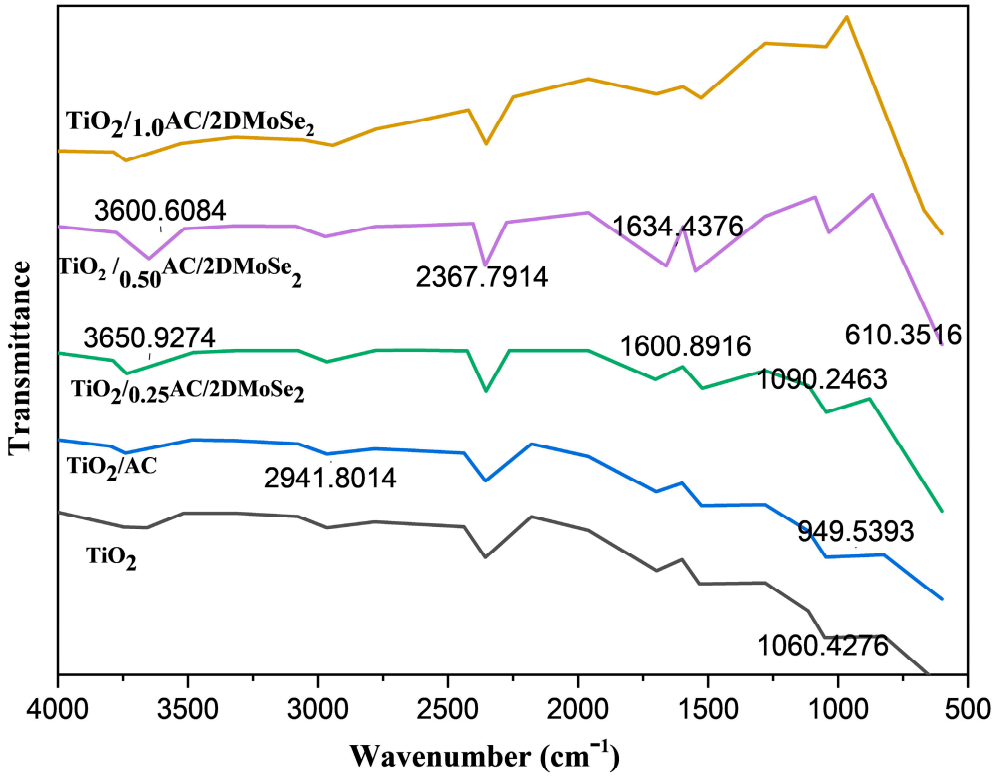

Figure 4. FTIR patterns: Pure TiO_2, TiO_2/AC and TiO_2/$_x$AC/2DMoSe_2 composite.

3.2. Structural Properties

The XRD spectra of synthesized composites are shown (Figure 5). These spectra were recorded at the National Center of Excellence in Physical Chemistry Labs, University of Peshawar Pakistan, by using a diffractometer (X-ray diffractometer, model. JDX-3532, JEOL, Tokyo Japan) using X-rays; CuKα CuKα (λ = 1.5418 Å), 2θ = 0 to 160°.

The crystal structure of synthesized photocatalysts were characterized by XRD. It is clear from the spectrum that there is no prominent difference in the diffraction peaks of pure TiO_2 and synthesized photocatalyst nano composites (Figure 5). It clarifies that the incorporation of activated carbon and 2D$MoSe_2$ has a negligible effect on the crystal structure of TiO_2. Due to a small amount of $MoSe_2$ and its high dispersion power on the surface of activated carbon and TiO_2, no prominent peak of $MoSe_2$ appeared in the XRD

spectrum of the composites [69,70]. Due to the amorphous nature of AC and less diffracting 2D material, no signals of activated carbon were found in the spectrum of photocatalyst [71]. Ammonium ions from ammonium molybdate easily enter into the layers of $MoSe_2$. These ammonium ions between the layers of $MoSe_2$ result in shifting of the peak to 9.25° [69,72]. The anatase structure of TiO_2 is indicated by (101) plane. The (110) plane represents the rutile TiO_2. As the percentage of AC increases the crystallinity of composites decreases successively. As a result, the intensity of peaks decreases gradually.

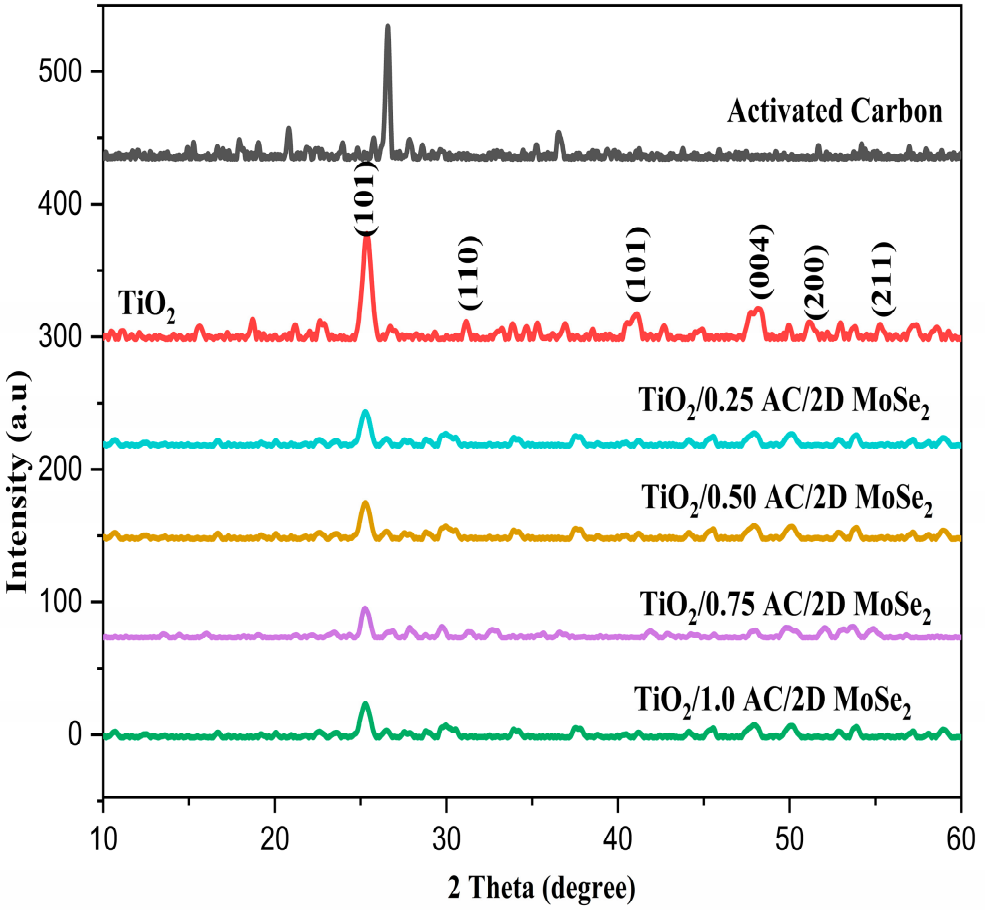

Figure 5. XRD patterns with different composition of AC in TiO_2/xAC/2D$MoSe_2$.

3.3. Morphological Properties

SEM photographs of synthesized photocatalysts are shown in Figure 6. Unfortunately, the SEM that we had in access, did not have high enough resolution to accurately characterize such small materials, but the pictures we captured were not a total failure, as demonstrated in Figure 6. Figure 6 show evidence of pristine $MoSe_2$ nanostructures on the surfaces of TiO_2 particles, and agglomerates are round by seeming, suggesting that they are made up of skinny, non-linear units. Pure activated carbon does not exhibit any crystalline shape as shown in Figure 6a. The spherical shape of pure TiO_2 nanocrystals appears in Figure 6b. This spherical shape in transformed into semi-spherical shape due to addition of activated carbon. Activated carbon surrounds a large surface area over TiO_2 nanocrystals [73,74]. Decrease in particle size of TiO_2 is an indication of even distribution of activated carbon in TiO_2 nanocrystals [75]. In the 2D $MoSe_2$ lattice structure, two layers of Se atoms sandwich the Mo atom. Weak van der Waals interaction between these layers develops a few-layered structures of 2D $MoSe_2$, known as the monolayer structure [76]. These monolayers of 2D $MoSe_2$ affect the crystalline structure of TiO_2 to some extent. From Figure 6c–f, an increasing percentage of activated carbon reduces the spherical shape of TiO_2 and the monolayer structure of 2D $MoSe_2$.

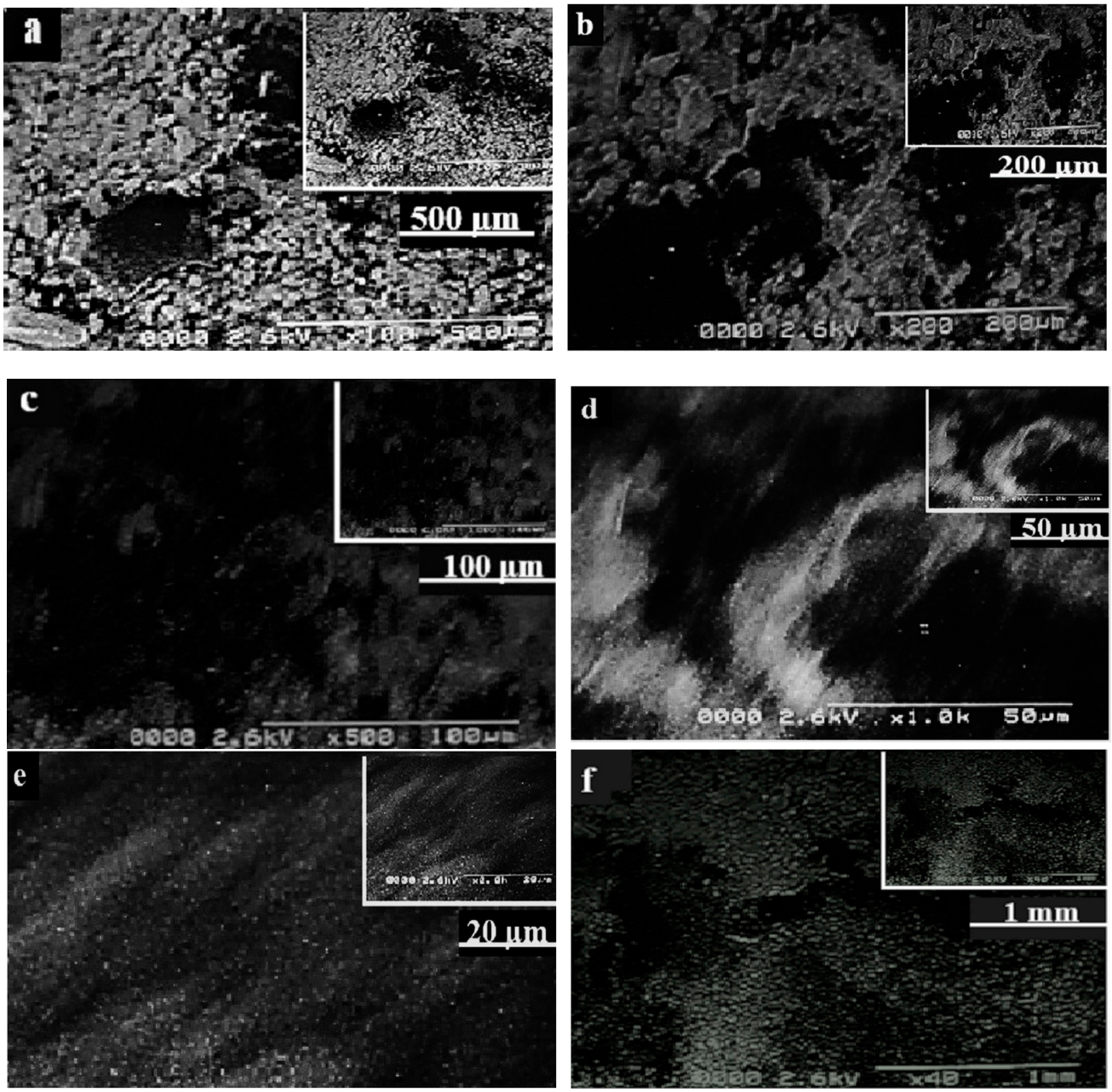

Figure 6. SEM images, (**a**) Pure AC; (**b**) Pure TiO_2 and (**c**–**f**) TiO_2/xAC/2D$MoSe_2$ composites.

3.4. Optical Properties

The results of the degradation of methylene blue dye are shown in Figures 7–11. 10 mg/L Methylene blue (MB) solution was used by catalyst loading of 0.1 g/dm^3 to evaluate efficiency of composites [77] 0.01 M $NaBH_4$ solution. The organic dye was selected as it shows color change as a result of degradation. This color change is the visual evidence of completion of photocatalytic chemical reaction. Being a member of the class cationic thiazine dye MB is widely known by its biochemical and chemical applications. MB shows a deep blue color in the aqueous solution in its oxidized form and is colorless in its reduced form [78]. MB shows absorption at 290 nm because of π to π^* transitions while at 664 nm because of n to π^* electronic shifting. These wavelengths help to monitor dye reduction [79]. $NaBH_4$ is well known due to its strong reducing property. It was used in dye solution, in such an extent that its low redox potential cannot complete the reaction and kinetically show forbidden behavior [80].

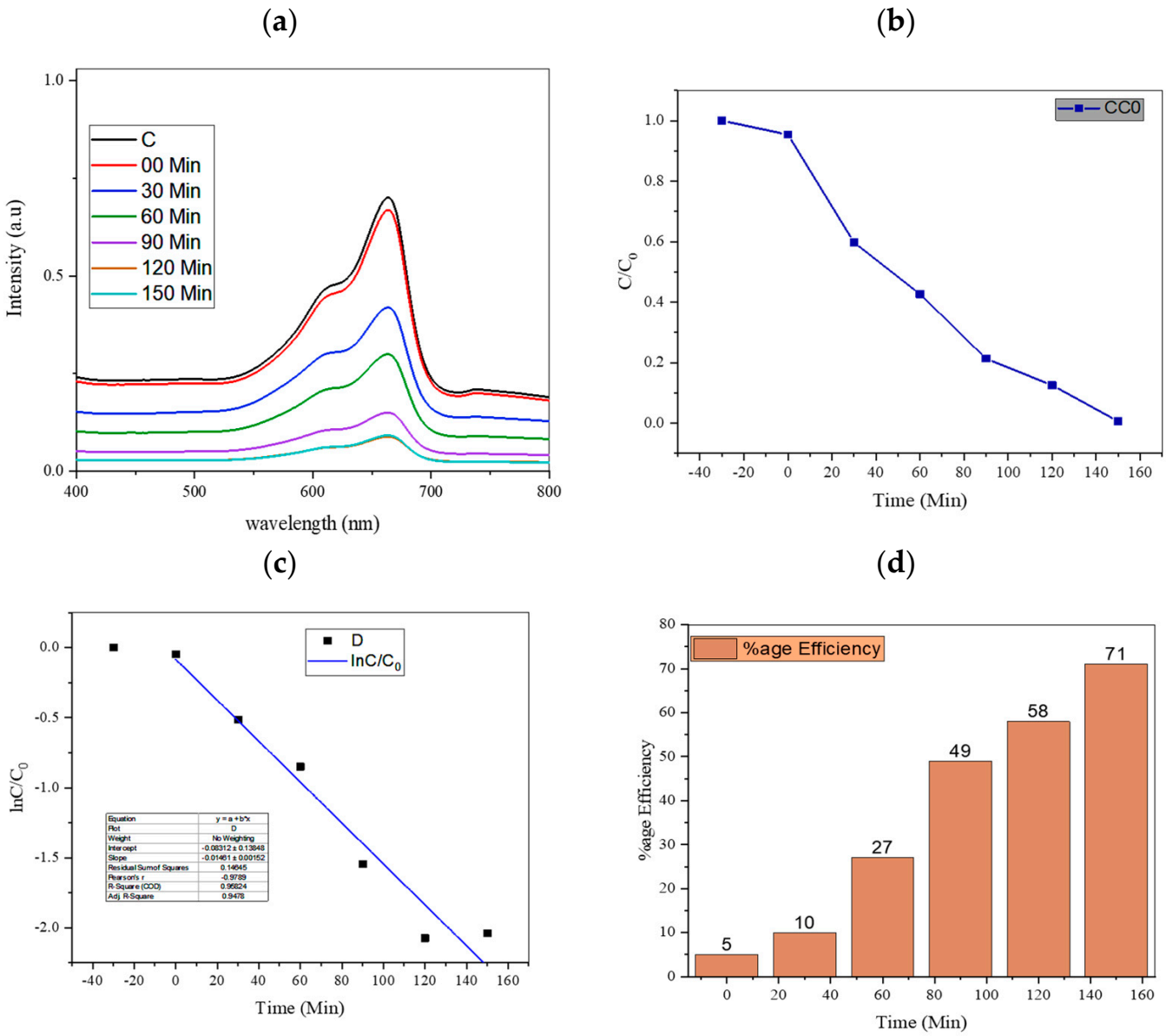

Figure 7. Photocatalytic degradation of Pure TiO_2: (**a**) Degradation of MB at different time intervals; (**b**) C/C_0 against time; (**c**) ln C/C_0 against time; (**d**) %age Efficiency.

In the first step, the photocatalytic activity of synthesized composites was examined by degrading methylene blue in aqueous solution. In the absence of photocatalysts in blank solution, a very small change appeared in the color and intensity after 150 min. This shows that $NaBH_4$, individually has no tendency to degrade dye. However, in the presence of a small amount of photocatalysts, a significant increase in dye degradation appeared.

The degradation of methylene blue was achieved by adding 1 mL of $NaBH_4$ (0.001 M) in 50 mL of 10 µg/L dye solution by constant stirring. A sample from this solution was taken as the standard. After 5 min, 15 mg of photocatalyst was added into solution. The prepared mixture was kept under dark for 150 min. Samples were taken out from the reaction mixture at 30 min intervals to study the effect of time on degradation of MB. After that, Philips light emitting Diode (LED) of 24 W was used to irradiate the solution keeping approximately 10 cm away from it to examine the photocatalytic degradation efficiency of synthesized composites. The LED lamp emits radiations of $\lambda > 400$ nm. The stirring of the solution continued until the completion of the reaction. A small volume of the sample was

taken out from the reaction mixture at 30 min intervals for the kinetic studies of the MB degradation using UV-visible spectroscopy.

The process is repeated for all the synthesized composites in order to study their photocatalytic behavior. Photocatalytic degradation of MB was repeated three times under the same conditions to perform the re-usability test of the synthesized photocatalysts. All the experiments were performed in 150 min. The photocatalytic efficiency of synthesized composites was calculated by applying the following formula:

$$\text{Percentage efficiency} = \frac{C_0 - C}{C_0} \times 100 \quad (1)$$

where C_0 = concentration of MB solution before photocatalytic reaction; C = concentration of MB solution after photo irradiation for given time t.

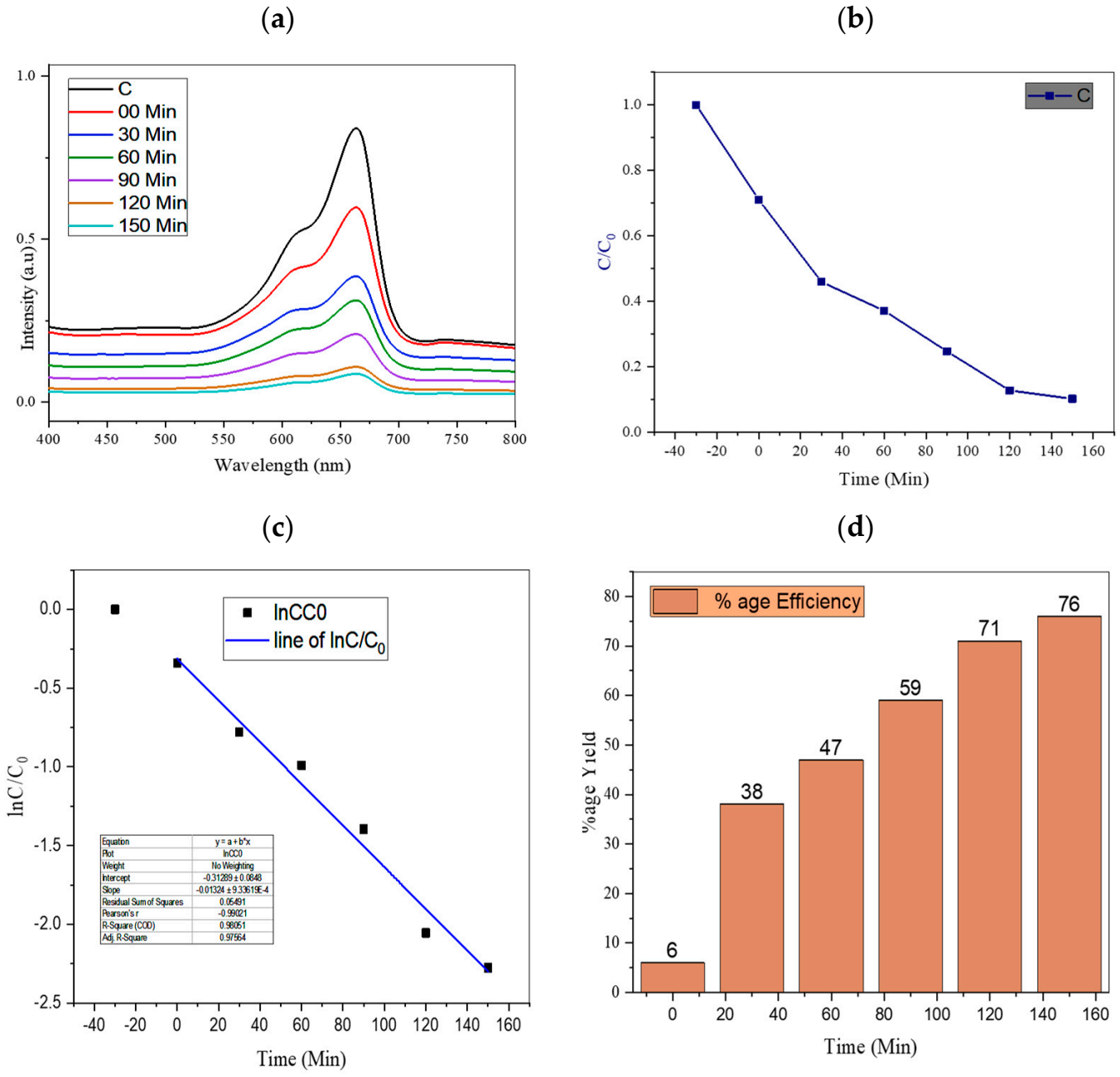

Figure 8. Photocatalytic degradation of TiO_2/0.25AC/2D$MoSe_2$: (**a**) Degradation of MB at different time intervals; (**b**) C/C_0 against time; (**c**) ln C/C_0 against time; (**d**) %age Efficiency.

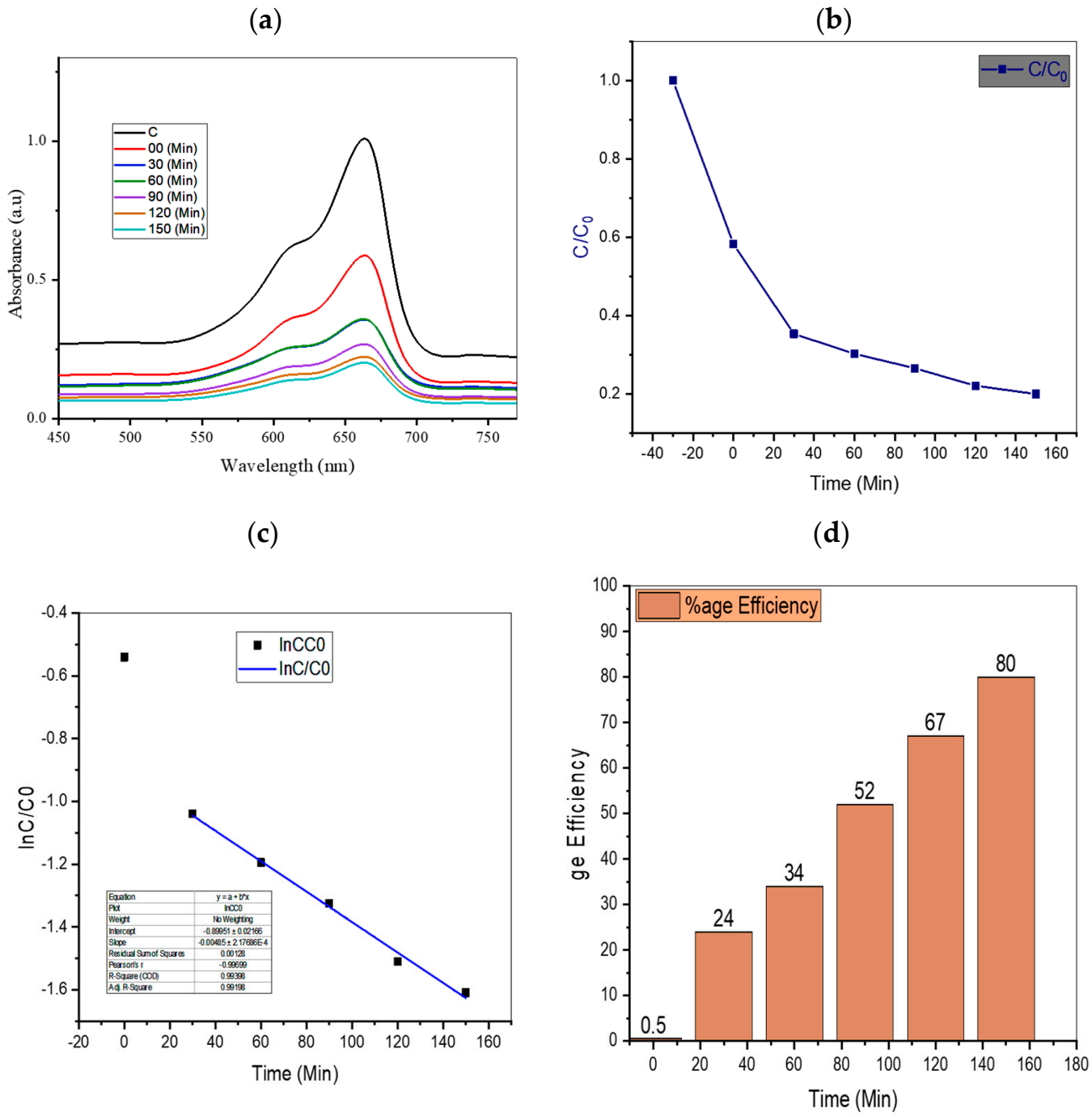

Figure 9. Photocatalytic degradation of $TiO_2/_{0.5}AC/2DMoSe_2$: (**a**) Degradation of MB at different time intervals; (**b**) C/C_0 against time; (**c**) ln C/C_0 against time; (**d**) %age Efficiency.

Figure 7a shows the photocatalytic degradation of pure TiO_2 while Figures 8a, 9a, 10a and 11a shows the photocatalytic degradation of synthesized composites having MB with the passage of time. From these results, it is clear that the photocatalyst with the higher percentage of AC in composite shows the maximum absorption of light and maximum degradation efficiency.

The effect of light irradiation time on the MB concentration ratio (C/C_0) is shown in Figures 7b, 8b, 9b, 10b and 11b. C and C_0 are the initial concentrations of MB in and concentrations at time t, in the aqueous phase. The C/C_0 ratio makes a convenient visual comparison of the photocatalytic effect of the composite.

On the base of the Langmuir–Hinshelwood model, photocatalytic reactions show pseudo first order kinetics. The first order rate constant k can be calculated by applying formula:

$$\ln C/C_0 = -kt \quad (2)$$

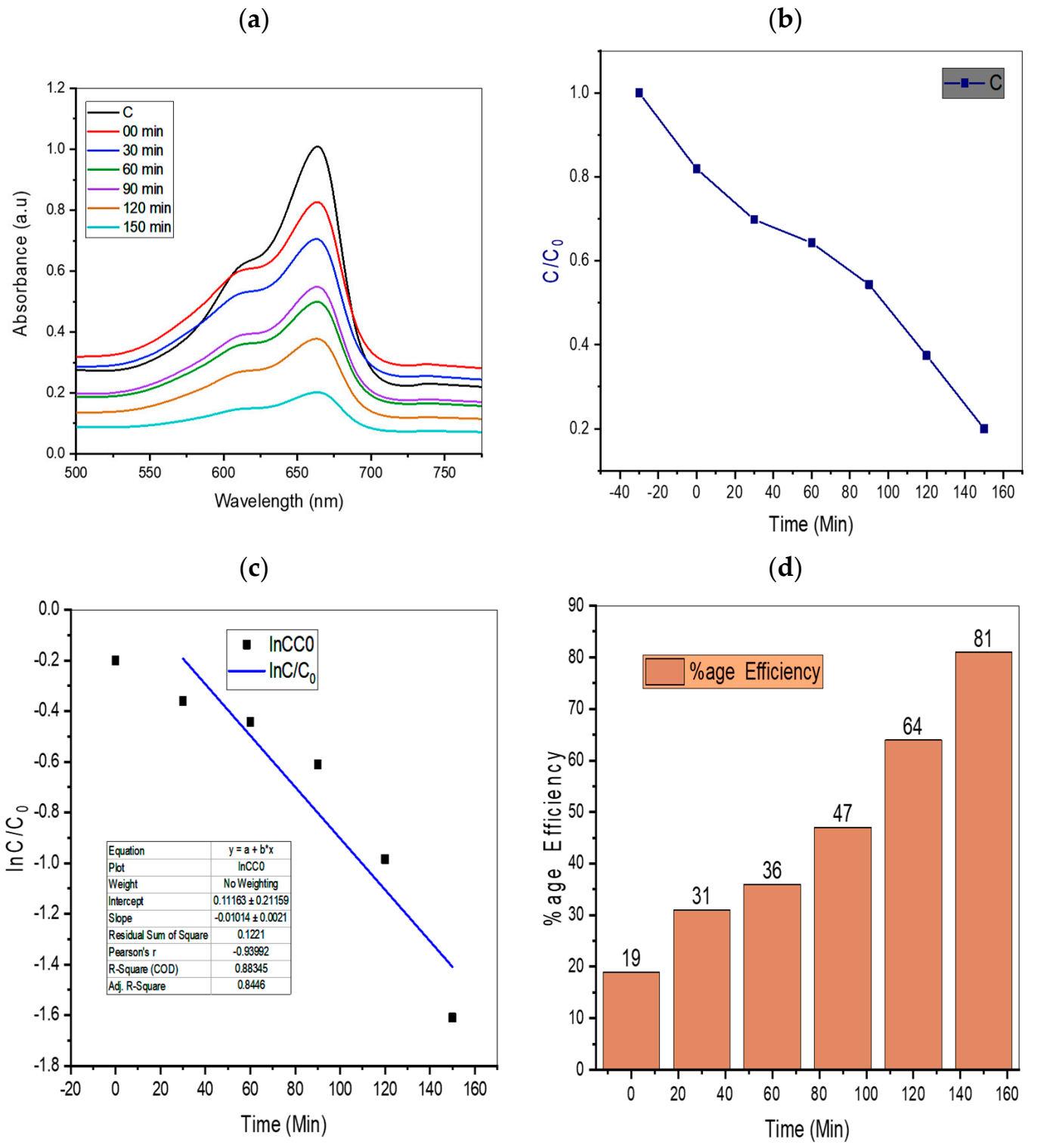

Figure 10. Photocatalytic degradation of $TiO_2/_{0.75}AC/2DMoSe_2$: (**a**) Degradation of MB at different time intervals; (**b**) C/C_0 against time; (**c**) ln C/C_0 against time; (**d**) %age Efficiency.

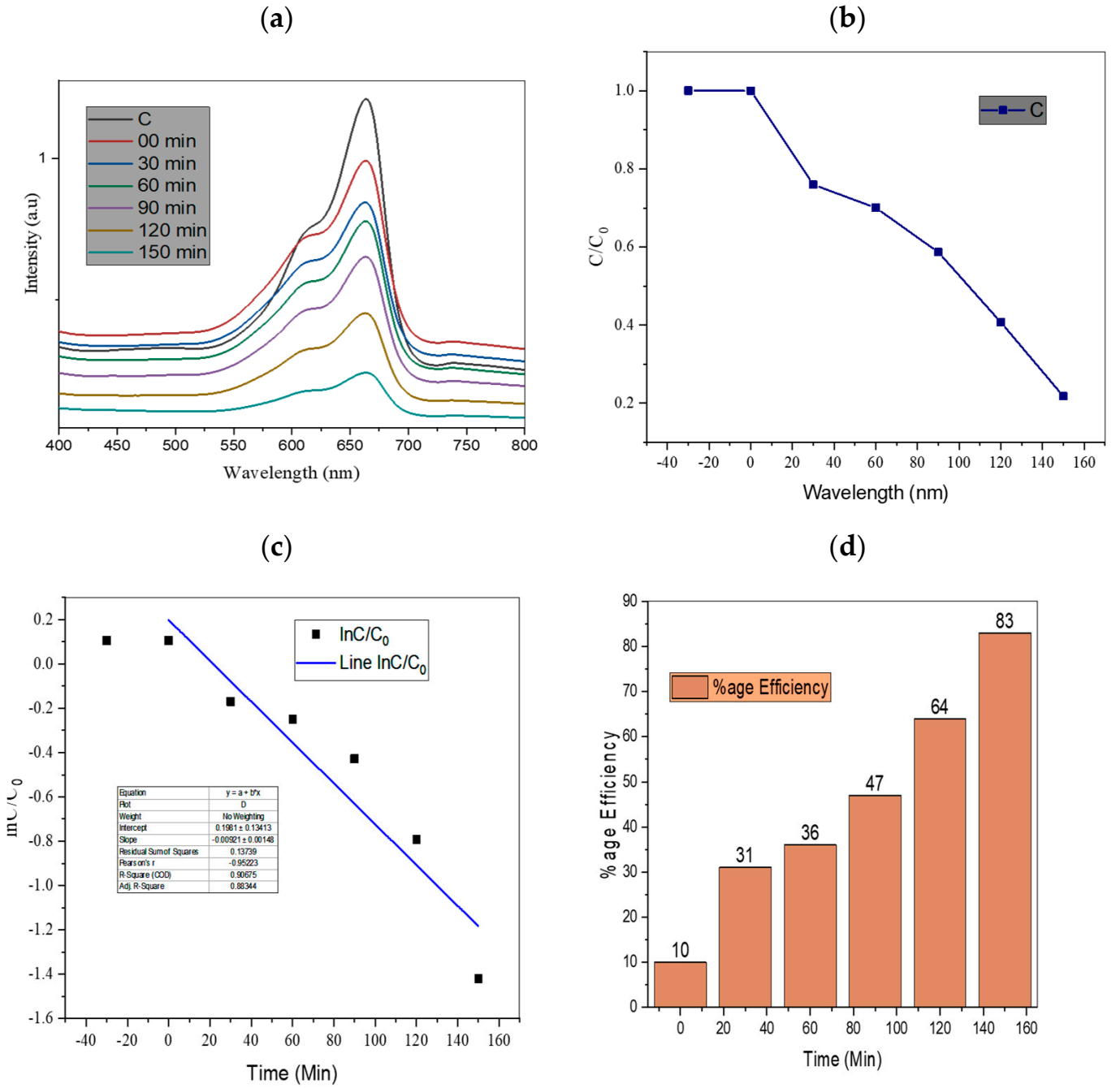

Figure 11. Photocatalytic degradation of $TiO_2/_1AC/2DMoSe_2$: (**a**) Degradation of MB at different time intervals; (**b**) C/C_0 against time; (**c**) ln C/C_0 against time; (**d**) %age efficiency.

Figures 7c, 8c, 9c, 10c and 11c show that pure TiO_2 and synthesized photocatalytic composites show pseudo-first order kinetics.

The percentage of degradation efficiency of pure TiO_2 and synthesized composites is shown in Figures 7d, 8d, 9d, 10d and 11d. From these graphical representations it is clear that increased amounts of AC in composites increases the light absorption capability of the photocatalyst which in turn results in increased photocatalytic activity.

Pure TiO_2 shows the absorption maximum at 390 nm. It shows that TiO_2 works only in the ultraviolet region. Pure $MoSe_2$ shows remarkable absorption in the ultraviolet, visible and infrared region [79]. $TiO_2/_xAC/2D$ $MoSe_2$ show absorption in the visible to infrared region. A large distribution of pore size structures in the photocatalyst, due to the presence

of activated carbon and 2D $MoSe_2$ will make it able to absorb all the ultraviolet, visible and near infrared light.

Table 2 shows the comparative % efficiency of AC, TiO_2 alone, combinations of TiO_2 with AC and CNTs and our synthesized TiO_2/AC/2D $MoSe_2$ to degrade MB. From the literature, it was found that the degradation efficiency of TiO_2 and activated carbon is not high when we use these materials individually to degrade organic pollutants in wastewater [81,82]. The degradation efficiency of activated carbon is only 55%. The degradation property of activated carbon is due to the presence of active sites on its surface. The light absorption power of pure TiO_2 decreases with the passage of time, so it showed 73% degradation at 30 minutes' interval. Incorporation of activated carbon with TiO_2 increased light absorption behavior of photocatalyst [68]. In another study, TiO_2@AC showed 65% degradation of MB in 180 min. The Xenon lamp was used as a light source for the degradation of MB in that study [75]. Askari et al., (2017) decorated TiO_2 with multi-walled carbon nano tubes (MWCNT) and used synthesized photocatalyst for the degradation of MB dye in water. The UV Philip lamp was used as a radiation source in that study. The photocatalyst showed 61.1% degradation of MB at the rate of 30 min [83]. Yoon, C.-J., et al., (2021) developed the TiO_2@carbon nanotube and evaluated the photocatalytic activity of the TiO_2@carbon nanotube photocatalyst by the degradation of MB in water. The photocatalyst showed 85% degradation of MB when the UV radiation source was used [84]. Alghamdi, Y.G., et al., (2022) synthesized biomass based activated carbon loaded with TiO_2 and used it for the photocatalytic degradation of oflxacin and reactive red 120. The photocatalyst showed 82% degradation in the UV light source [85]. Justh et al., (2019) studied the photocatalytic properties of TiO_2@carbon aerogel composites. Composites were prepared using the atomic layer deposition method. Photocatalysts showed 55% degradation at 240 min interval [86]. All the above studies show that TiO_2 along with AC absorbs light in the ultraviolet region. Although carbon nano-tubes and activated carbon increased the photocatalytic activity of TiO_2 up to 85%, these composites required ultraviolet light for photodegradation. A main portion of sunlight is composed of the visible light spectrum.

Table 2. Comparison of photodegradation efficiencies of previously studied and synthesized composites.

Sr. No.	Composite	Ratio	Photodegradation %Age Efficiency
1	AC	pure	55% [75]
2	TiO_2	Pure	71–73% [75]
3	TiO_2/AC	NA	55% [86]
4	TiO_2@AC	NA	65% [87]
5	TiO_2/MWCNT	NA	61.1% [83]
6	TiO_2@carbon nanotube	NA	85% [84]
7	AC-TiO_2/(OFL)	NA	82% [85]
8	TiO_2/AC/2D $MoSe_2$	1:0.25:1	76% present work
9	TiO_2/AC/2D $MoSe_2$	1:0.5:1	80% present work
10	TiO_2/AC/2D $MoSe_2$	1:0.75:1	81% present work
11	TiO_2/AC/2D $MoSe_2$	1:1:1	83% present work

In the present study, 2D $MoSe_2$ was incorporated in TiO_2/AC to reduce the band gap of TiO_2 and to increase the absorption spectrum of composites in the visible and NIR region. From the values given in Table 2, it is also clear that the increased amount of AC proved effective in increasing the efficiency of the photocatalyst as it increases the light absorption capacity of the composite. The results show that maximum efficiency of synthesized nanocomposite was observed with the increase in ratio of AC. The maximum degradation efficiency (83%) of TiO_2/AC/2D $MoSe_2$ was observed at maximum ratio of AC i.e., 1:1:1. The increase in light absorbance decreases dye intensity in water with the passage of time. As time increases, the absorbance of light decreases which indicates that dye molecules are dissociating into their fragments. The photocatalytic activity of the synthesized composites is due to the reduced band gap of TiO_2 because of the presence

of $2DMoSe_2$ and the enhanced light absorption property due to the presence of elemental activated carbon.

4. Parameters Affecting Photodegradation of Methylene Blue

4.1. Effect of Irradiation Time

The effect of time of irradiation on dye degradation was studied by successive increase in time intervals irradiation on the MB samples in the presence of photocatalysts as shown in Table 3. As the reaction time increases, a decrease in the absorption peak of MB appears. At the same time, the color changes from blue to colorless. The reason for the decrease in the absorption spectra is reduction of MB chromophore.

Table 3. Effect of irradiation time on MB degradation using photocatalysts.

Photocatalyst	Time (min)	0	30	60	90	120	150
Pure TiO_2	MB mg/L	10	9	7.3	5.1	4.2	2.9
$TiO_2/_{0.25}AC/2DMoSe_2$		10	6.2	5.3	4.1	2.9	2.4
$TiO_2/_{0.50}AC/2DMoSe_2$		10	7.6	6.6	4.8	3.3	2.0
$TiO_2/_{0.75}AC/2DMoSe_2$		10	7.0	6.5	5.5	3.5	1.9
$TiO_2/AC/2DMoSe_2$		10	6.9	6.4	5.3	3.6	1.7

4.2. Effect of Initial Dye Concentration

To study the effect of initial concentration of MB on degradation rate, aqueous solution of MB was prepared with concentration 5 mg/L, 10 mg/L, 15 mg/L, 20 mg/L and 25 mg/L. The maximum percentage degradation shown by the photocatalyst, "$TiO_2/AC/2DMoSe_2$", is given in the Table 4.

Table 4. Initial concentration of MB versus percentage degradation.

Sr. No.	MB (mg/L)	% Degradation
1	5	87
2	10	83
3	15	74
4	20	69
6	25	65

The nature of dye, its initial concentration and presence of foreign species in the dye solution greatly affect the rate of photodegradation [88]. At a lower concentration of MB, its absorption capacity is high. It is because of the availability of more active sites on the surface of the photocatalyst for low MB concentration [89]. Active sites of the photocatalyst are covered by higher adsorption of dye molecules which decreases the photodegradation rate at a higher concentration of MB. A higher concentration of dye molecule increases the screening effect of light and minimizes the production of $^{\bullet}OH$ active radicals [90]. In the present study, the degradation rate of MB was found to be high at a lower concentration of MB.

4.3. Effect of pH

To determine the impact of pH, MB solutions with different pH values were used. A little change in degradation was observed when pH is changed from 7.0 to 4.0 (Table 5). Degradation efficiency further decreased when pH decreased further from 4.0 to 2.0. While an increase in degradation was observed when the pH of the MB solution increased from 7 to 9.5. The maximum degradation efficiency was achieved after 120 min of irradiation.

MB absorbs on highly negative charged photocatalysts, as it is a cationic dye [91]. At a high pH (in basic medium), photocatalysts try to gain a negative charge which results in increased adsorption of positively charged dyes. This increased adsorption of dye on the surface of the photocatalyst is due to attraction of oppositely charged ions [92]. In acidic medium (at lower pH), positive ions of dye compete with H^+ of the medium, that results in

a decrease in adsorption on the surface of photocatalyst and a decrease in photodegradation. Similar is the case of MB dye. Reduction in the adsorption of MB on photocatalysts' surface reduces reaction between MB and •OH. There is no repulsion between MB and OH^- and repulsion between the negative surface of the photocatalyst and OH^-. As a result, OH^- will remain in reaction medium and play its vital role in the photodegradation process [93,94]. Jia et al., (2017), in a photocatalytic study of TiO_2, revealed that maximum absorption of MB on its surface takes place in basic medium. That was because of the electrostatic attraction between cationic dye on the negatively charged active surface of TiO_2 [95].

Table 5. Effect of change of pH on photodegradation.

Sr. No.	pH	Percentage Degradation
1	7.0	72
2	7.5	74
3	8.0	79
4	8.5	80
5	9.0	82
6	9.5	83
7	10.0	81

4.4. Effect of Catalyst Loading

It is necessary to find out the optimum quantity of the photocatalyst for optimum photodegradation of MB. The effect of catalyst loading on the photodegradation of MB was checked by irradiating UV/Visible radiations and keeping other parameters constant. The amount of photocatalyst varied from 0.01 g/dm^3 to 0.25 g/dm^3 for 5 ppm MB solution. Photodegradation efficiency is shown in Table 6. It can be seen from the data that degradation efficiency increases as the amount of catalyst increases and then decreases.

Table 6. Effect of catalyst load on photodegradation efficiency.

Sr. No.	Catalyst Loading (g/dm^3)	Percentage Degradation
1	0.01	79
2	0.10	83
3	0.15	73
4	0.20	66
5	0.25	62

After the optimum amount of photocatalyst, further increase in the amount results in agglomeration. At higher levels of concentration turbidity of solution also increases. These two factors inhibit the absorption of photons on the surface of the photocatalyst and decrease its efficiency [96].

5. Proposed Photocatalytic Mechanism

From the Figure 12, it is clear that the energy band gap of $MoSe_2$ was found to be 1.80 eV, so it can cover a broad solar energy region. The flat-band potential of $MoSe_2$ was found to be 2.27 V on NHE. The photocatalytic mechanism of the synthesized composite is shown in the figure schematically. When light falls on the photocatalyst, valence band electrons of TiO_2 are transferred to the conduction band leaving holes in the valence band. These valence electrons of TiO_2 can be transferred to the conduction band of $MoSe_2$ as it lies nearer to the VB of TiO_2 as compared to its conduction band. 2D $MoSe_2$ sheets act as active sites to carry out reactions. Separation of photogenerated electrons and reduction of charge recombination becomes easy in such heterostructures, which leads to efficient and enhanced photocatalytic activity. The adjustable band gap improves the light absorption range in the visible region of the composite. As the photocatalytic activity of the sample is linked with visible light absorption, 2D $MoSe_2$ improves the activity of TiO_2 in the visible

region and near the IR region. In addition to this, activated carbon enhances the absorption capacity of the composite.

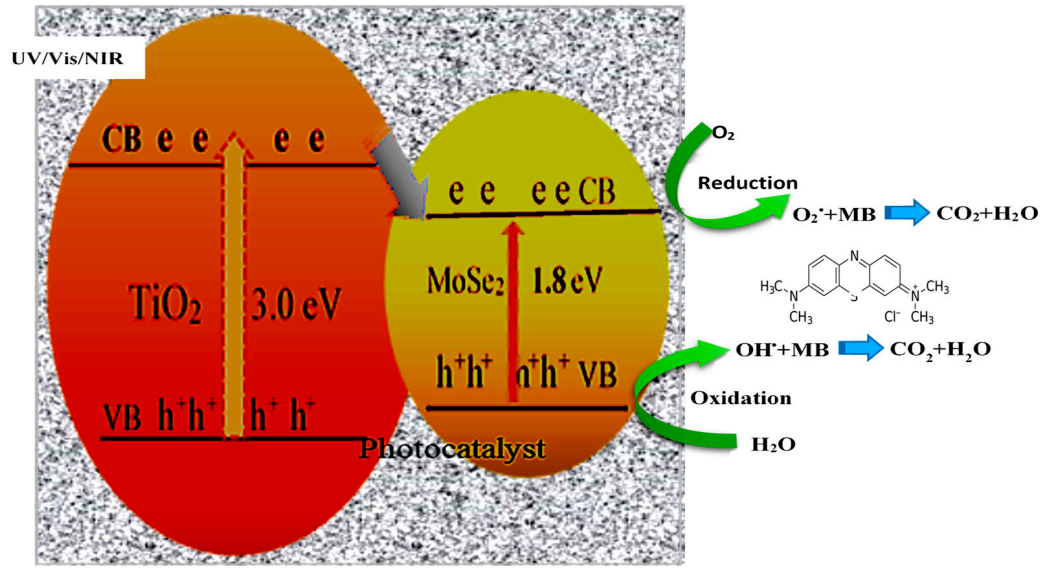

Figure 12. Proposed mechanism of action of TiO_2/AC/2D$MoSe_2$ photocatalyst.

Photochemical reactions involved in degradation of dye are given below.

$$\text{Photoexcitation: } TiO_2/AC/2D\ MoSe_2 + hv\ (TiO_2\ \text{surface}) \rightarrow e^-_{CB}TiO_2 + h^+_{VB}TiO_2 \quad (3)$$

$$\text{Entrapment of free electrons: } e^-_{CB}\ (TiO_2) \rightarrow e^-_{CB}\ (MoSe_2) \quad (4)$$

$$\text{Photoexcited electron scavenging (Reduction): } (O_2)_{ads} + e^-_{CB}(MoSe_2) \rightarrow O^{\bullet}_2 \quad (5)$$

$$\text{Decomposition reaction: } MB + O^{\bullet}_2 \rightarrow CO_2 + H_2O \quad (6)$$

$$\text{Entrapment of holes: } h^+_{VB}(TiO_2) \rightarrow h^+_{VB}\ (MoSe_2) \quad (7)$$

$$\text{Oxidation of hydroxyls: } OH + h^+_{VB}\ (MoSe_2) \rightarrow OH^{\bullet} \quad (8)$$

$$\text{Photodegradation by OH• radicals: } MB + OH^{\bullet} \rightarrow CO_2 + H_2O \quad (9)$$

The above reactions describe details of the photocatalytic degradation process. Pollutants transfer from the bulk of wastewater to the surface of the photocatalyst. Adsorption of pollutants on the surface of the photocatalyst is activated by photons of light. Photons of light (UV-Vis-NIR region) excite electrons from the valence band of TiO_2 to its conduction band and produce holes on the valence band of TiO_2. Photo-excited electrons migrate from the conduction band of TiO_2 to the conduction band of $MoSe_2$. These electrons reduce molecular oxygen into oxygen free radicals. Being very reactive, these oxygen free radicals decompose organic pollutants such as MB into carbon dioxide gas and water molecules. Holes generated as a result of photo-excitation move from the valence band of TiO_2 to the valence band of $MoSe_2$. These holes oxidize water molecules into $^{\bullet}OH$. These $^{\bullet}OH$ are involved in the decomposition of organic pollutants. Decomposition products of this reaction are CO_2 and H_2O. After these reactions, $^{\bullet}O_2$ and OH could be generated by entrapped UV-Vis-NIR light. These free radicals are strong oxidizing agents and can easily decompose organic pollutants present in wastewater.

6. Conclusions

Composites of TiO_2 with 2D $MoSe_2$ were synthesized in two steps and then AC was incorporated in these composites. The simple hydrothermal method was used for this purpose. TiO_2 nanocrystals were synthesized from titanium tetrabutoxide in NaOH solution. Nanocrystals were calcinated at a high 300 °C for 3 h to obtain a stable phase of TiO_2 nanoparticles. $2DMoSe_2$ was prepared by using sodium selenite and ammonium paramolybdate tetrahydrate. $TiO_2/_xAC/2DMoSe_2$ composites were synthesized with the addition of AC and TiO_2 in the reaction mixture of sodium selenite and ammonium paramolybdate tetrahydrate. The synthesis and morphology of $TiO_2/_xAC/2DMoSe_2$ composites were established by FTIR, XRD and SEM. UV—vis spectroscopy and FT-IR analysis indicated the successful stabilization of composites. The studies revealed that composites are very useful as active photocatalysts to degrade MB and are expected to be equally useful to degrade other organic pollutants present in wastewater in the visible light spectrum. The extended activity of synthesized composites credited to the anatase-phase of TiO_2 facilitated with the narrow-band gap 2D $MoSe_2$. Moreover, the presence of AC in the composite helps to absorb extended solar radiation which resulted in an increase in photocatalytic activity of composites. As the percentage of AC increases in composites, degradation power increased directly. The environment-friendly synthesis of $TiO_2/_xAC/2DMoSe_2$ using simple aqueous medium is an encouraging proposal to prepare composites of other metals as well. Photocatalytic composites can be used efficiently to fight with different environmental pitfalls including toxic organic dyes and health hazardous organic pollutants present in industrial wastewater. Synthesized composites showed maximum (83%) degradation efficiency that is greater than the degradation efficiency of any individual semiconductor i.e., TiO_2 and 2D $MoSe_2$ and previously reported TiO_2 based photocatalysts. This indicates a very useful application of synthesized nano composites in industrial water treatments.

Author Contributions: Conceptualization, M.S.T.; Methodology, M.B.T.; Validation, M.S.; Formal analysis, S.A.; Investigation, M.B.T.; Resources, G.M.K., X.Z. and B.J.; Data curation, M.S.; Writing—original draft, S.A.; Writing—review & editing, S.N.; Visualization, S.N.; Supervision, M.S.T. and G.M.K.; Funding acquisition, X.Z. and B.J. All authors have read and agreed to the published version of the manuscript.

Funding: This research was funded by the National Natural Science Foundation of China at the Chinese Academy of Science and the APC was funded by Grant numbers 21974149 and 22174152.

Data Availability Statement: All data included in this study are available upon request by contacting the corresponding author.

Conflicts of Interest: The authors declare no conflict of interest.

References

1. Krishna, R.; Mishra, J.; Ighalo, J.O. Rising demand for rain water harvesting system in the world: A case study of Joda Town, India. *World Sci. News* **2020**, *146*, 47–59.
2. Olvera, R.C.; Silva, S.L.; Robles-Belmont, E.; Lau, E.Z. Review of nanotechnology value chain for water treatment applications in Mexico. *Resour.-Effic. Technol.* **2017**, *3*, 1–11. [CrossRef]
3. Singha, I.; Mishrab, P.K. Nano-membrane filtration a novel application of nanotechnology for waste water treatment. *Mater. Today Proc.* **2020**, *29*, 327–332. [CrossRef]
4. Kamali, M.; Persson, K.M.; Costa, M.E.; Capela, I. Sustainability criteria for assessing nanotechnology applicability in industrial wastewater treatment: Current status and future outlook. *Environ. Int.* **2019**, *125*, 261–276. [CrossRef]
5. Das, A.; Dey, A. P-Nitrophenol-Bioremediation using potent *Pseudomonas* strain from the textile dye industry effluent. *J. Environ. Chem. Eng.* **2020**, *8*, 103830. [CrossRef]
6. Anas, M.; Han, D.S.; Mahmoud, K.; Park, H.; Abdel-Wahab, A. Photocatalytic degradation of organic dye using titanium dioxide modified with metal and non-metal deposition. *Mater. Sci. Semicond. Process.* **2016**, *41*, 209–218. [CrossRef]
7. de Vidales, M.J.M.; Nieto-Márquez, A.; Morcuende, D.; Atanes, E.; Blaya, F.; Soriano, E.; Fernández-Martínez, F. 3D printed floating photocatalysts for wastewater treatment. *Catal. Today* **2019**, *328*, 157–163. [CrossRef]
8. Ighalo, J.O.; Adeniyi, A.G.; Adeniran, J.A.; Ogunniyi, S. A systematic literature analysis of the nature and regional distribution of water pollution sources in Nigeria. *J. Clean. Prod.* **2021**, *283*, 124566. [CrossRef]

9. Kumar, S.; Ahlawat, W.; Bhanjana, G.; Heydarifard, S.; Nazhad, M.M.; Dilbaghi, N. Nanotechnology-based water treatment strategies. *J. Nanosci. Nanotechnol.* **2014**, *14*, 1838–1858. [CrossRef]
10. Qu, X.; Brame, J.; Li, Q.; Alvarez, P.J. Nanotechnology for a safe and sustainable water supply: Enabling integrated water treatment and reuse. *Acc. Chem. Res.* **2013**, *46*, 834–843. [CrossRef]
11. Nwabor, O.F.; Nnamonu, E.; Martins, P.; Ani, O. Water and waterborne diseases: A review. *Int. J. Trop. Dis. Health* **2016**, *12*, 1–14.
12. Munir, H.M.S.; Feroze, N.; Ramzan, N.; Sagir, M.; Babar, M.; Tahir, M.S.; Shamshad, J.; Mubashir, M.; Khoo, K.S. Fe-zeolite catalyst for ozonation of pulp and paper wastewater for sustainable water resources. *Chemosphere* **2022**, *297*, 134031. [CrossRef] [PubMed]
13. Chen, L.; Caro, F.; Corbett, C.J.; Ding, X. Estimating the environmental and economic impacts of widespread adoption of potential technology solutions to reduce water use and pollution: Application to China's textile industry. *Environ. Impact Assess. Rev.* **2019**, *79*, 106293. [CrossRef]
14. Mittal, H.; Kumar, A.; Khanuja, M. In-situ oxidative polymerization of aniline on hydrothermally synthesized $MoSe_2$ for enhanced photocatalytic degradation of organic dyes. *J. Saudi Chem. Soc.* **2019**, *23*, 836–845. [CrossRef]
15. Khan, S.; Malik, A. Environmental and health effects of textile industry wastewater. In *Environmental Deterioration and Human Health*; Springer: Berlin/Heidelberg, Germany, 2014; pp. 55–71.
16. Tounsadi, H.; Metarfi, Y.; Taleb, M.; El Rhazi, K.; Rais, Z. Impact of chemical substances used in textile industry on the employee's health: Epidemiological study. *Ecotoxicol. Environ. Saf.* **2020**, *197*, 110594. [CrossRef]
17. Bener, S.; Atalay, S.; Ersöz, G. The hybrid process with eco-friendly materials for the treatment of the real textile industry wastewater. *Ecol. Eng.* **2020**, *148*, 105789. [CrossRef]
18. Gupta, R.; Pandit, C.; Pandit, S.; Gupta, P.K.; Lahiri, D.; Agarwal, D.; Pandey, S. Potential and future prospects of biochar-based materials and their applications in removal of organic contaminants from industrial wastewater. *J. Mater. Cycles Waste Manag.* **2022**, *24*, 852–876. [CrossRef]
19. Jaganathan, V.; Cherurveettil, P.; Chellasamy, A.; Premapriya, M. Environmental pollution risk analysis and management in textile industry: A preventive mechanism. In Proceedings of the 1st International Conference on Social Sciences and Humanities, ICSH 2014, Gaborone, Botswana, 4–7 June 2014.
20. Khan, I.; Saeed, K.; Zekker, I.; Zhang, B.; Hendi, A.H.; Ahmad, A.; Ahmad, S.; Zada, N.; Ahmad, H.; Shah, L.A. Review on methylene blue: Its properties, uses, toxicity and photodegradation. *Water* **2022**, *14*, 242. [CrossRef]
21. Santoso, E.; Ediati, R.; Kusumawati, Y.; Bahruji, H.; Sulistiono, D.; Prasetyoko, D. Review on recent advances of carbon based adsorbent for methylene blue removal from waste water. *Mater. Today Chem.* **2020**, *16*, 100233. [CrossRef]
22. Abdelrahman, E.A.; Hegazey, R.; El-Azabawy, R.E. Efficient removal of methylene blue dye from aqueous media using Fe/Si, Cr/Si, Ni/Si, and Zn/Si amorphous novel adsorbents. *J. Mater. Res. Technol.* **2019**, *8*, 5301–5313. [CrossRef]
23. Shandilya, P.; Mittal, D.; Soni, M.; Raizada, P.; Hosseini-Bandegharaei, A.; Saini, A.K.; Singh, P. Fabrication of fluorine doped graphene and $SmVO_4$ based dispersed and adsorptive photocatalyst for abatement of phenolic compounds from water and bacterial disinfection. *J. Clean. Prod.* **2018**, *203*, 386–399. [CrossRef]
24. Raizada, P.; Sudhaik, A.; Singh, P.; Shandilya, P.; Saini, A.K.; Gupta, V.K.; Lim, J.-H.; Jung, H.; Hosseini-Bandegharaei, A. Fabrication of Ag_3VO_4 decorated phosphorus and sulphur co-doped graphitic carbon nitride as a high-dispersed photocatalyst for phenol mineralization and *E. coli* disinfection. *Sep. Purif. Technol.* **2019**, *212*, 887–900. [CrossRef]
25. Pare, B.; Singh, P.; Jonnalgadda, S. *Degradation and Mineralization of Victoria Blue B Dye in a Slurry Photoreactor Using Advanced Oxidation Process*; CSIR: New Delhi, India, 2009.
26. Pare, B.; Singh, P.; Jonnalagadda, S. *Visible Light Induced Heterogeneous Advanced Oxidation Process to Degrade Pararosanilin Dye in Aqueous Suspension of ZnO*; CSIR: New Delhi, India, 2008.
27. Watanabe, N.; Nakamura, S.; Liu, B.; Wang, N. Utilization of Structure from Motion for processing CORONA satellite images: Application to mapping and interpretation of archaeological features in Liangzhu Culture, China. *Archaeol. Res. Asia* **2017**, *11*, 38–50. [CrossRef]
28. Sharma, K.; Dutta, V.; Sharma, S.; Raizada, P.; Hosseini-Bandegharaei, A.; Thakur, P.; Singh, P. Recent advances in enhanced photocatalytic activity of bismuth oxyhalides for efficient photocatalysis of organic pollutants in water: A review. *J. Ind. Eng. Chem.* **2019**, *78*, 1–20. [CrossRef]
29. Priya, B.; Raizada, P.; Singh, N.; Thakur, P.; Singh, P. Adsorptional photocatalytic mineralization of oxytetracycline and ampicillin antibiotics using Bi_2O_3/BiOCl supported on graphene sand composite and chitosan. *J. Colloid Interface Sci.* **2016**, *479*, 271–283. [CrossRef]
30. Raizada, P.; Singh, P.; Kumar, A.; Pare, B.; Jonnalagadda, S.B. Zero valent iron-brick grain nanocomposite for enhanced solar-Fenton removal of malachite green. *Sep. Purif. Technol.* **2014**, *133*, 429–437. [CrossRef]
31. Sudhaik, A.; Raizada, P.; Shandilya, P.; Singh, P. Magnetically recoverable graphitic carbon nitride and $NiFe_2O_4$ based magnetic photocatalyst for degradation of oxytetracycline antibiotic in simulated wastewater under solar light. *J. Environ. Chem. Eng.* **2018**, *6*, 3874–3883. [CrossRef]
32. Raizada, P.; Kumari, J.; Shandilya, P.; Dhiman, R.; Singh, V.P.; Singh, P. Magnetically retrievable Bi_2WO_6/Fe_3O_4 immobilized on graphene sand composite for investigation of photocatalytic mineralization of oxytetracycline and ampicillin. *Process Saf. Environ. Prot.* **2017**, *106*, 104–116. [CrossRef]
33. Chen, D.; Cheng, Y.; Zhou, N.; Chen, P.; Wang, Y.; Li, K.; Huo, S.; Cheng, P.; Peng, P.; Zhang, R. Photocatalytic degradation of organic pollutants using TiO_2-based photocatalysts: A review. *J. Clean. Prod.* **2020**, *268*, 121725. [CrossRef]

34. Jafari, S.; Zhao, F.; Zhao, D.; Lahtinen, M.; Bhatnagar, A.; Sillanpää, M. A comparative study for the removal of methylene blue dye by N and S modified TiO_2 adsorbents. *J. Mol. Liq.* **2015**, *207*, 90–98. [CrossRef]
35. Beiki, H.; Esfahany, M.N.; Etesami, N. Turbulent mass transfer of Al_2O_3 and TiO_2 electrolyte nanofluids in circular tube. *Microfluid. Nanofluid.* **2013**, *15*, 501–508. [CrossRef]
36. Kusiak-Nejman, E.; Morawski, A.W. TiO_2/graphene-based nanocomposites for water treatment: A brief overview of charge carrier transfer, antimicrobial and photocatalytic performance. *Appl. Catal. B Environ.* **2019**, *253*, 179–186. [CrossRef]
37. Lee, C.-G.; Javed, H.; Zhang, D.; Kim, J.-H.; Westerhoff, P.; Li, Q.; Alvarez, P.J. Porous electrospun fibers embedding TiO_2 for adsorption and photocatalytic degradation of water pollutants. *Environ. Sci. Technol.* **2018**, *52*, 4285–4293. [CrossRef] [PubMed]
38. Mallakpour, S.; Nikkhoo, E. Surface modification of nano-TiO_2 with trimellitylimido-amino acid-based diacids for preventing aggregation of nanoparticles. *Adv. Powder Technol.* **2014**, *25*, 348–353. [CrossRef]
39. Raza, N.; Raza, W.; Gul, H.; Azam, M.; Lee, J.; Vikrant, K.; Kim, K.-H. Solar-light-active silver phosphate/titanium dioxide/silica heterostructures for photocatalytic removal of organic dye. *J. Clean. Prod.* **2020**, *254*, 120031. [CrossRef]
40. Alamelu, K.; Ali, B.J. Au nanoparticles decorated sulfonated graphene-TiO_2 nanocomposite for sunlight driven photocatalytic degradation of recalcitrant compound. *Sol. Energy* **2020**, *211*, 1194–1205. [CrossRef]
41. Moradi, M.; Khorasheh, F.; Larimi, A. Pt nanoparticles decorated Bi-doped TiO_2 as an efficient photocatalyst for CO_2 photo-reduction into CH_4. *Sol. Energy* **2020**, *211*, 100–110. [CrossRef]
42. Xie, Z.; Zhao, F.; Zou, S.; Zhu, F.; Zhang, Z.; Wang, W. TiO_2 nanorod arrays decorated with Au nanoparticles as sensitive and recyclable SERS substrates. *J. Alloy. Compd.* **2021**, *861*, 157999. [CrossRef]
43. Xiao, W.-Z.; Xu, L.; Rong, Q.-Y.; Dai, X.-Y.; Cheng, C.-P.; Wang, L.-L. Two-dimensional H-TiO_2/MoS_2 (WS_2) van der Waals heterostructures for visible-light photocatalysis and energy conversion. *Appl. Surf. Sci.* **2020**, *504*, 144425. [CrossRef]
44. Wang, S.; Yun, J.-H.; Luo, B.; Butburee, T.; Peerakiatkhajohn, P.; Thaweesak, S.; Xiao, M.; Wang, L. Recent progress on visible light responsive heterojunctions for photocatalytic applications. *J. Mater. Sci. Technol.* **2017**, *33*, 1–22. [CrossRef]
45. Yang, L.; Hao, X.; Yu, D.; Zhou, P.; Peng, Y.; Jia, Y.; Zhao, C.; He, J.; Zhan, C.; Lai, B. High visible-light catalytic activity of Bis-PDI-T@ TiO_2 for activating persulfate toward efficient degradation of carbamazepine. *Sep. Purif. Technol.* **2021**, *263*, 118384. [CrossRef]
46. Kang, L.; Zhang, M.; Zhang, J.; Liu, S.; Zhang, N.; Yao, W.; Ye, Y.; Luo, C.; Gong, Z.; Wang, C. Dual-defect surface engineering of bimetallic sulfide nanotubes towards flexible asymmetric solid-state supercapacitors. *J. Mater. Chem. A* **2020**, *8*, 24053–24064. [CrossRef]
47. Wang, S.; Li, Y.; Wang, X.; Zi, G.; Zhou, C.; Liu, B.; Liu, G.; Wang, L.; Huang, W. One-step supramolecular preorganization constructed crinkly graphitic carbon nitride nanosheets with enhanced photocatalytic activity. *J. Mater. Sci. Technol.* **2022**, *104*, 155–162. [CrossRef]
48. Wu, L.; Shi, S.; Li, Q.; Zhang, X.; Cui, X. TiO_2 nanoparticles modified with 2D $MoSe_2$ for enhanced photocatalytic activity on hydrogen evolution. *Int. J. Hydrog. Energy* **2019**, *44*, 720–728. [CrossRef]
49. Hu, Z.; Wu, Z.; Han, C.; He, J.; Ni, Z.; Chen, W. Two-dimensional transition metal dichalcogenides: Interface and defect engineering. *Chem. Soc. Rev.* **2018**, *47*, 3100–3128. [CrossRef]
50. Wang, D.; Xu, Y.; Sun, F.; Zhang, Q.; Wang, P.; Wang, X. Enhanced photocatalytic activity of TiO_2 under sunlight by MoS2 nanodots modification. *Appl. Surf. Sci.* **2016**, *377*, 221–227. [CrossRef]
51. Liang, Z.; Bai, X.; Hao, P.; Guo, Y.; Xue, Y.; Tian, J.; Cui, H. Full solar spectrum photocatalytic oxygen evolution by carbon-coated TiO_2 hierarchical nanotubes. *Appl. Catal. B Environ.* **2019**, *243*, 711–720. [CrossRef]
52. Coehoorn, R.; Haas, C.; Dijkstra, J.; Flipse, C.d.; De Groot, R.; Wold, A. Electronic structure of $MoSe_2$, MoS_2, and WSe_2. I. Band-structure calculations and photoelectron spectroscopy. *Phys. Rev. B* **1987**, *35*, 6195. [CrossRef]
53. Boyjoo, Y.; Sun, H.; Liu, J.; Pareek, V.K.; Wang, S. A review on photocatalysis for air treatment: From catalyst development to reactor design. *Chem. Eng. J.* **2017**, *310*, 537–559. [CrossRef]
54. Ren, Z.; Liu, X.; Zhuge, Z.; Gong, Y.; Sun, C.Q. $MoSe_2$/ZnO/ZnSe hybrids for efficient Cr (VI) reduction under visible light irradiation. *Chin. J. Catal.* **2020**, *41*, 180–187. [CrossRef]
55. Rivera, P.; Schaibley, J.R.; Jones, A.M.; Ross, J.S.; Wu, S.; Aivazian, G.; Klement, P.; Seyler, K.; Clark, G.; Ghimire, N.J. Observation of long-lived interlayer excitons in monolayer $MoSe_2$–WSe_2 heterostructures. *Nat. Commun.* **2015**, *6*, 6242. [CrossRef] [PubMed]
56. Chen, J.; Liu, B.; Cai, H.; Liu, S.; Yamauchi, Y.; Jun, S.C. Covalently Interlayer-Confined Organic–Inorganic Heterostructures for Aqueous Potassium Ion Supercapacitors. *Small* **2023**, *19*, 2204275. [CrossRef] [PubMed]
57. Xie, T.; Liu, Y.; Wang, H.; Wu, Z. Layered $MoSe_2$/Bi_2WO_6 composite with PN heterojunctions as a promising visible-light induced photocatalyst. *Appl. Surf. Sci.* **2018**, *444*, 320–329. [CrossRef]
58. Leary, R.; Westwood, A. Carbonaceous nanomaterials for the enhancement of TiO_2 photocatalysis. *Carbon* **2011**, *49*, 741–772. [CrossRef]
59. Yan, Y.; Kuang, W.; Shi, L.; Ye, X.; Yang, Y.; Xie, X.; Shi, Q.; Tan, S. Carbon quantum dot-decorated TiO_2 for fast and sustainable antibacterial properties under visible-light. *J. Alloy. Compd.* **2019**, *777*, 234–243. [CrossRef]
60. Moosavi, S.; Lai, C.W.; Gan, S.; Zamiri, G.; Akbarzadeh Pivehzhani, O.; Johan, M.R. Application of efficient magnetic particles and activated carbon for dye removal from wastewater. *ACS Omega* **2020**, *5*, 20684–20697. [CrossRef]
61. Siddiqui, I.; Mittal, H.; Kohli, V.K.; Gautam, P.; Ali, M.; Khanuja, M. Hydrothermally synthesized micron sized, broom-shaped $MoSe_2$ nanostructures for superior photocatalytic water purification. *Mater. Res. Express* **2018**, *5*, 125020. [CrossRef]

62. Pan, J.; Zhu, X.; Chen, X.; Zhao, Y.; Liu, J. Gd^{3+}-Doped $MoSe_2$ nanosheets used as a theranostic agent for bimodal imaging and highly efficient photothermal cancer therapy. *Biomater. Sci.* **2018**, *6*, 372–387. [CrossRef]
63. Subramani, A.; Byrappa, K.; Kumaraswamy, G.; Ravikumar, H.; Ranganathaiah, C.; Lokanatha Rai, K.; Ananda, S.; Yoshimura, M. Hydrothermal preparation and characterization of TiO_2: AC composites. *Mater. Lett.* **2007**, *61*, 4828–4831. [CrossRef]
64. Alkorbi, A.S.; Javed, H.M.A.; Hussain, S.; Latif, S.; Mahr, M.S.; Mustafa, M.S.; Alsaiari, R.; Alhemiary, N.A. Solar light-driven photocatalytic degradation of methyl blue by carbon-doped TiO_2 nanoparticles. *Opt. Mater.* **2022**, *127*, 112259. [CrossRef]
65. Thinkohkaew, K.; Piroonpan, T.; Jiraborvornpongsa, N.; Potiyaraj, P. Development of multifunctional polypropylene nonwoven fabric by radiation induced grafting of TiO_2 nanoparticles and trifluoroethyl methacrylate for protective textile applications. *Materialia* **2022**, *21*, 101355. [CrossRef]
66. Jimoh, A.; Akpeji, B.; Azeez, S.; Ayipo, Y.; Abdulsalam, Z.; Adebayo, Z.; Ajao, A.; Zakariyah, A.; Elemike, E. Biosynthesis of Ag and TiO_2 nanoparticles and the evaluation of their antibacterial activities. *Inorg. Chem. Commun.* **2022**, *141*, 109503. [CrossRef]
67. Dessai, S.; Ayyanar, M.; Amalraj, S.; Khanal, P.; Vijayakumar, S.; Gurav, N.; Rarokar, N.; Kalaskar, M.; Nadaf, S.; Gurav, S. Bioflavonoid mediated synthesis of TiO_2 nanoparticles: Characterization and their biomedical applications. *Mater. Lett.* **2022**, *311*, 131639. [CrossRef]
68. Liu, S.; Chen, X.; Chen, X. A TiO_2/AC composite photocatalyst with high activity and easy separation prepared by a hydrothermal method. *J. Hazard. Mater.* **2007**, *143*, 257–263. [CrossRef] [PubMed]
69. Cai, Q.; Wang, F.; Xiang, J.; Dan, M.; Yu, S.; Zhou, Y. Layered MoS_2 Grown on Anatase TiO_2 {001} Promoting Interfacial Electron Transfer to Enhance Photocatalytic Evolution of H_2 From H_2S. *Front. Environ. Chem.* **2020**, *1*, 591645. [CrossRef]
70. Yuan, Y.-J.; Ye, Z.-J.; Lu, H.-W.; Hu, B.; Li, Y.-H.; Chen, D.-Q.; Zhong, J.-S.; Yu, Z.-T.; Zou, Z.-G. Constructing anatase TiO_2 nanosheets with exposed (001) facets/layered MoS2 two-dimensional nanojunctions for enhanced solar hydrogen generation. *ACS Catal.* **2016**, *6*, 532–541. [CrossRef]
71. Wang, S.; Yi, L.; Halpert, J.E.; Lai, X.; Liu, Y.; Cao, H.; Yu, R.; Wang, D.; Li, Y. A novel and highly efficient photocatalyst based on P25–graphdiyne nanocomposite. *Small* **2012**, *8*, 265–271. [CrossRef]
72. Dashora, A.; Ahuja, U.; Venugopalan, K. Electronic and optical properties of MoS_2 (0 0 0 1) thin films: Feasibility for solar cells. *Comput. Mater. Sci.* **2013**, *69*, 216–221. [CrossRef]
73. Mohammad, N.H.; EL-Sherbiny, G.M.; Hammad, A.A.; Askar, A.A.; El-Nour, S.A.A. Gamma-ray and sunlight-induced synthesis of silver nanoparticles using bacterial cellulose and cell-free filtrate produced by Komagataeibacter rhaeticus N1 MW322708 strain. *Cellulose* **2022**, *29*, 1791–1805. [CrossRef]
74. Shah, I.H.; Ashraf, M.; Sabir, I.A.; Manzoor, M.A.; Malik, M.S.; Gulzar, S.; Ashraf, F.; Iqbal, J.; Niu, Q.; Zhang, Y. Green synthesis and Characterization of Copper oxide nanoparticles using Calotropis procera leaf extract and their different biological potentials. *J. Mol. Struct.* **2022**, *1259*, 132696. [CrossRef]
75. Parvathiraja, C.; Katheria, S.; Siddiqui, M.R.; Wabaidur, S.M.; Islam, M.A.; Lai, W.-C. Activated Carbon-Loaded Titanium Dioxide Nanoparticles and Their Photocatalytic and Antibacterial Investigations. *Catalysts* **2022**, *12*, 834. [CrossRef]
76. Dai, C.; Zhou, Z.; Tian, C.; Li, Y.; Yang, C.; Gao, X.; Tian, X. Large-scale synthesis of graphene-like $MoSe_2$ nanosheets for efficient hydrogen evolution reaction. *J. Phys. Chem. C* **2017**, *121*, 1974–1981. [CrossRef]
77. Tichapondwa, S.M.; Newman, J.; Kubheka, O. Effect of TiO_2 phase on the photocatalytic degradation of methylene blue dye. *Phys. Chem. Earth Parts A/B/C* **2020**, *118*, 102900. [CrossRef]
78. Small, J.M.; Hintelmann, H. Methylene blue derivatization then LC–MS analysis for measurement of trace levels of sulfide in aquatic samples. *Anal. Bioanal. Chem.* **2007**, *387*, 2881–2886. [CrossRef]
79. Joseph, S.; Mathew, B. Microwave-assisted green synthesis of silver nanoparticles and the study on catalytic activity in the degradation of dyes. *J. Mol. Liq.* **2015**, *204*, 184–191. [CrossRef]
80. Al-Hamoud, K.; Shaik, M.R.; Khan, M.; Alkhathlan, H.Z.; Adil, S.F.; Kuniyil, M.; Assal, M.E.; Al-Warthan, A.; Siddiqui, M.R.H.; Tahir, M.N. Pulicaria undulata Extract-Mediated Eco-Friendly Preparation of TiO_2 Nanoparticles for Photocatalytic Degradation of Methylene Blue and Methyl Orange. *ACS Omega* **2022**, *7*, 4812–4820. [CrossRef]
81. Rahman, Q.I.; Ali, A.; Ahmad, N.; Lohani, M.B.; Mehta, S.; Muddassir, M. Synthesis and characterization of CuO rods for enhanced visible light driven dye degradation. *J. Nanosci. Nanotechnol.* **2020**, *20*, 7716–7723. [CrossRef]
82. Rahman, Q.I.; Hasan, S.; Ali, A.; Mehta, S.; Raja, M.A.; Ahmad, N.; Khan, A.R.; Muddassir, M. Synthesis and Characterizations of Nitrogen (N) Doped Strontium Titanate ($SrTiO_3$) Nanoparticles for Enhanced Visible Light Driven Photocatalytic Degradation. *J. Nanosci. Nanotechnol.* **2020**, *20*, 6475–6481. [CrossRef]
83. Askari, M.B.; Banizi, Z.T.; Seifi, M.; Dehaghi, S.B.; Veisi, P. Synthesis of TiO_2 nanoparticles and decorated multi-wall carbon nanotube (MWCNT) with anatase TiO_2 nanoparticles and study of optical properties and structural characterization of TiO_2/MWCNT nanocomposite. *Optik* **2017**, *149*, 447–454. [CrossRef]
84. Yoon, C.-J.; Lee, S.-H.; Kwon, Y.-B.; Kim, K.; Lee, K.-H.; Kim, S.M.; Kim, Y.-K. Fabrication of sustainable and multifunctional TiO_2@ carbon nanotube nanocomposite fibers. *Appl. Surf. Sci.* **2021**, *541*, 148332. [CrossRef]
85. Alghamdi, Y.G.; Krishnakumar, B.; Malik, M.A.; Alhayyani, S. Design and preparation of biomass-derived activated carbon loaded TiO_2 photocatalyst for photocatalytic degradation of reactive red 120 and ofloxacin. *Polymers* **2022**, *14*, 880. [CrossRef] [PubMed]

86. Justh, N.; Mikula, G.J.; Bakos, L.P.; Nagy, B.; László, K.; Parditka, B.; Erdélyi, Z.; Takáts, V.; Mizsei, J.; Szilágyi, I.M. Photocatalytic properties of TiO_2@ polymer and TiO_2@ carbon aerogel composites prepared by atomic layer deposition. *Carbon* **2019**, *147*, 476–482. [CrossRef]
87. Saravanan, L.; Patil, R.A.; Gultom, P.; Kumar, B.; Manikandan, A.; Fu, Y.-P.; Chueh, Y.-L.; Cheng, C.-L.; Yeh, W.-C.; Ma, Y.-R. Rutile-phase TiO_2@ carbon core-shell nanowires and their photoactivation in visible light region. *Carbon* **2021**, *181*, 280–289. [CrossRef]
88. Salama, A.; Mohamed, A.; Aboamera, N.M.; Osman, T.; Khattab, A. Photocatalytic degradation of organic dyes using composite nanofibers under UV irradiation. *Appl. Nanosci.* **2018**, *8*, 155–161. [CrossRef]
89. Elsayed, E.M.; Elnouby, M.S.; Gouda, M.; Elessawy, N.A.; Santos, D. Effect of the morphology of tungsten oxide embedded in sodium alginate/polyvinylpyrrolidone composite beads on the photocatalytic degradation of methylene blue dye solution. *Materials* **2020**, *13*, 1905. [CrossRef]
90. Abdellah, M.; Nosier, S.; El-Shazly, A.; Mubarak, A. Photocatalytic decolorization of methylene blue using TiO_2/UV system enhanced by air sparging. *Alex. Eng. J.* **2018**, *57*, 3727–3735. [CrossRef]
91. Azeez, F.; Al-Hetlani, E.; Arafa, M.; Abdelmonem, Y.; Nazeer, A.A.; Amin, M.O.; Madkour, M. The effect of surface charge on photocatalytic degradation of methylene blue dye using chargeable titania nanoparticles. *Sci. Rep.* **2018**, *8*, 7104. [CrossRef]
92. Nguyen Thi Thu, T.; Nguyen Thi, N.; Tran Quang, V.; Nguyen Hong, K.; Nguyen Minh, T.; Le Thi Hoai, N. Synthesis, characterisation, and effect of pH on degradation of dyes of copper-doped TiO_2. *J. Exp. Nanosci.* **2016**, *11*, 226–238. [CrossRef]
93. Hejazi, R.; Mahjoub, A.R.; Khavar, A.H.C.; Khazaee, Z. Fabrication of novel type visible-light-driven TiO_2@ MIL-100 (Fe) microspheres with high photocatalytic performance for removal of organic pollutants. *J. Photochem. Photobiol. A Chem.* **2020**, *400*, 112644. [CrossRef]
94. Hendekhale, N.R.; Mohammad-Khah, A. A novel synthesis of Co_2ZrO_5 and m-ZrO_2 nanoparticles by sono-precipitation and hydrothermal methods and their application in UV/Visible-photocatalytic studies. *J. Environ. Chem. Eng.* **2020**, *8*, 104065. [CrossRef]
95. Jia, Z.; La, L.; Zhang, W.; Liang, S.; Jiang, B.; Xie, S.; Habibi, D.; Zhang, L. Strong enhancement on dye photocatalytic degradation by ball-milled TiO_2: A study of cationic and anionic dyes. *J. Mater. Sci. Technol.* **2017**, *33*, 856–863. [CrossRef]
96. Khade, G.; Gavade, N.; Suwarnkar, M.; Dhanavade, M.; Sonawane, K.; Garadkar, K. Enhanced photocatalytic activity of europium doped TiO_2 under sunlight for the degradation of methyl orange. *J. Mater. Sci. Mater. Electron.* **2017**, *28*, 11002–11011. [CrossRef]